

Properties of galaxy clusters in different cosmological scenarios. I. Intrinsic properties.

Pascal A.M. de Theije¹, Eelco van Kampen²*, Remco G. Slijkhuis¹

¹*Sterrewacht Leiden, P.O.Box 9513, 2300 RA Leiden, The Netherlands*

²*Royal Observatory Edinburgh, Blackford Hill, Edinburgh EH9 3HJ, Scotland*

Accepted ; Received ; in original form

ABSTRACT

We study the influence of the various parameters of scenarios of large-scale structure formation on properties of galaxy clusters, and investigate which cluster properties are most sensitive to these parameters. We present a set of large N-body simulations and derive the intrinsic properties of galaxy clusters in these simulations, which represent a volume of $256^3 h^{-3} \text{ Mpc}^3$. The cosmological scenarios studied differ in either the shape of the power spectrum of initial fluctuations, its normalization, the density parameter Ω_0 , or the Hubble parameter H_0 . The cluster properties that are studied are the mass, line-of-sight velocity dispersion, peculiar velocity, intrinsic shape, and orientation with respect to its surroundings.

The present-day *r.m.s.* mass fluctuation on scales of $8h^{-1} \text{ Mpc}$, σ_8 , which is largely determined by the normalization of the initial power spectrum, has a large impact on the cluster properties. The latter, viz. the cluster number density, mass, line-of-sight velocity dispersion and peculiar velocity, are also determined by Ω_0 , though somewhat less. Other parameters, such as H_0 , the tilt of the initial fluctuation spectrum, and the exact shape of this spectrum, are generally less important.

Unlike the other cluster properties studied, the peculiar velocity is found to depend on all parameters of the formation scenario.

In a companion paper the properties of the model clusters are compared to observations to try and discriminate between different cosmological scenarios. Using scaling relations between the average properties of the cluster sample and the parameters of the formation scenario, one may try and interpolate between the scenarios studied here in order to find the parameters of the scenario that is most consistent with the data.

Key words: Galaxies: clustering – cosmology: observations – large-scale structure in the Universe.

1 INTRODUCTION

As clusters of galaxies are the largest objects in the Universe that have recently collapsed, or are still collapsing, the properties of a representative sample of these can help constrain scenarios for large-scale structure formation in the Universe.

N-body simulations of large patches of the Universe were used extensively to compare the properties of the simulated clusters with observations. Frenk *et al.* (1990) calculated the distribution of velocity dispersions of clusters, identified both in 3-D and in 2-D. Jing & Fang (1994) determined the cumulative distributions of mass, velocity dispersion, temperature of clusters as well as their space density in three scenarios, viz. standard CDM, low- Ω_0 CDM, and a

hybrid of CDM and HDM. Jing & Börner (1995) determined the velocity dispersion profiles of clusters for seven cosmological scenarios. They found that the velocity dispersion profiles depend both on Ω_0 and on the cosmological constant Λ . The profiles are steeper in a low- Ω_0 scenario than for a high value of Ω_0 . This effect is weaker for a larger value of Λ . Mohr *et al.* (1995) carried out numerical simulations for three cosmological scenarios ($\Omega_0 = 1.0$, $\Omega_0 = 0.2$, $\Omega_0 = 0.2$ with $\lambda_0 = \Lambda/3H_0^2 = 0.8$) with an effective power spectrum $P(k) \propto k^{-1}$ on cluster scales. They compared the projected X-ray shapes of the clusters in these scenarios to the observed shapes. They favoured the $\Omega_0 = 1$ scenario, although the authors admitted that some discrepancies remain. De Theije *et al.* (1995) used the galaxy distribution of 99 clusters to determine the projected ellipticities, and compared these to the results of N-body simulations of van Kampen (1994). They found that in the $\Omega_0 = 1$ CDM scenario clus-

* Present address: Theoretical Astrophysics Center, Juliane Maries Vej 30, DK-2100 Copenhagen, Denmark

ters are too elongated with respect to real observed clusters. From a limited number of simulations for an $\Omega_0 = 0.2$ CDM model, they concluded that clusters in this scenario are generally more nearly spherical than for $\Omega_0 = 1.0$.

N-body simulations were also used to study cluster alignments. Dekel, West & Aarseth (1984) and West, Dekel & Oemler (1989) concluded that the orientations of clusters of galaxies with respect to their neighbours provide a sensitive test for the formation of large-scale structure in the Universe.

Many observational properties of clusters were studied in the recent past and much numerical work has been done. Most of the latter, however, concentrated on just one or two cluster properties. Also, in most studies up till now clusters were identified in the simulations in three dimensions, or background galaxies were not removed from the observations.

In order to improve upon this state of affairs, we have run a set of cosmological N-body simulations with the following goals: (1) Evaluate the intrinsic properties of the clusters, i.e., of the groups of particles defined in 3-D that fulfill certain constraints. (2) Investigate the influence of the cosmological parameters on the cluster properties and study which cluster properties are mostly affected by varying the cosmology. (3) Obtain scaling relations between the average properties of the cluster sample and the parameters of the formation scenario to allow interpolation between the studied scenarios. (4) Compare the cluster properties of the model clusters with observations. The results of this comparison, together with the results of other studies, e.g., of the fluctuations in the 3K-background measured by COBE, can then be used to find the parameters of the scenario that is most consistent with all data. For the best-fitting scenario, a cluster catalogue will be constructed later on, similar to the standard CDM catalogue of van Kampen & Katgert (1997), in which each cluster will be simulated individually at higher resolution.

The cosmological parameters that are varied between the different scenarios are the shape of the initial power spectrum, its amplitude which gives rise to the present *r.m.s.* mass fluctuation on scales of $8h^{-1}$ Mpc, σ_8 , the density in units of the critical density, Ω_0 , and the Hubble-parameter, H_0 . The values of the parameters are chosen such that very often one can compare two scenarios that differ by only one parameter value, so that the influence of that specific parameter on the cluster properties can be investigated.

The comparison with observations is done in a companion paper (de Theije, van Kampen & Slijkhuis 1997, hereafter Paper II). In that paper, we will try to mimic as closely as possible the observational way of defining a cluster, to make a reliable comparison.

The present paper is organized as follows: in Section 2 we describe the N-body simulations, and the identification of groups in the simulations. In Section 3 we give the number densities of clusters in the simulation boxes and compare these to the observations. In Section 4 we describe the intrinsic properties of the clusters in the simulations, viz. their mass, velocity dispersion, peculiar velocity, shape, and alignment with the surroundings. In Section 5 we compare the properties of clusters for different parameter values, which allows us to investigate the influence of a given parameter on

Table 1. Description of the cosmological scenarios that have been examined. The first column gives the acronym, which will be used throughout this paper to identify a scenario. SCDM indicates the Standard CDM scenario with $\Omega_0 = 1.0$ and $h = 0.5$. The various LCDM scenarios all have $\Omega_0 < 1.0$. hCDM denotes a scenario with $h = 0.3$, and TCDM is a tilted CDM scenario, having a slightly tilted initial spectrum. The second column gives the shape of the power spectrum. The CDM power spectrum is taken from Davis *et al.* (1985), the HDM one from Bardeen *et al.* (1986). Column 3 denotes the present-day *r.m.s.* mass fluctuation in spheres of $8h^{-1}$ Mpc. For the $\Omega_0 = 1.0$ scenarios, the values are the maximum values we investigate (see text). Column 4 gives the density parameter. Column 5 gives the Hubble-constant in units of $100 \text{ km s}^{-1} \text{ Mpc}^{-1}$. Column 6 gives the index of the primordial spectrum, where $n = 1.0$ denotes the Harrison-Zeldovich spectrum and $n = 0.8$ corresponds to a slightly tilted initial spectrum. Column 7 gives the implied present age of the Universe for each scenario.

scenario	Power Spectrum	σ_8	Ω_0	h	n	age (10^{10} yr)
SCDM	CDM	0.61	1.0	0.5	1.0	1.3
LCDMa	CDM	0.46	0.2	0.5	1.0	1.7
LCDMb	CDM	0.90	0.2	0.5	1.0	1.7
LCDMc	CDM	0.90	0.2	1.0	1.0	0.8
LCDMd	CDM	0.60	0.8	0.5	1.0	1.4
k^{-2}	k^{-2}	0.64	1.0	0.5	-2.0	1.3
hCDM	CDM	1.00	1.0	0.3	1.0	2.2
TCDM	CDM	0.60	1.0	0.5	0.8	1.3
HDM	HDM	1.00	1.0	1.0	1.0	0.7

the cluster properties. Finally, in Section 6 the main results are summarized and discussed.

2 METHODS

2.1 Simulations

The simulations are performed using a P^3M code (Bertschinger & Gelb 1991) in a box of $256^3 h^{-3} \text{ Mpc}^3$ with periodic boundary conditions and 128^3 mesh points. 128^3 particles are used, each with a mass of $2.22 \times 10^{12} \Omega_0 h^{-1} M_\odot$. Each simulation took about 25 hours of CPU-time on the Cray C90 of the SARA Computing Center in Amsterdam. A softening length of $0.2 h^{-1}$ Mpc (i.e., one tenth of a grid cell) is used. This value is the same as Frenk *et al.* (1990) adopted, and makes a comparison between both studies possible. The accuracy of the simulations is judged from the Layzer-Irvine cosmic energy equation (see Efstathiou *et al.* 1985). In all simulations, the integration constant of this equation changes less than 0.06% of the current potential energy at any stage of a run.

The parameters that define the simulations are given in Table 1. All simulations are done using the same random number seed to set up the initial conditions in order to remove cosmic variance from the comparison of the various scenarios. The initial conditions are evaluated at $z = 9$ by means of the Zeldovich approximation. For the CDM simulations we use the Davis *et al.* (1985) power spectrum. For the HDM simulation we use the Bardeen *et al.* (1986) power spectrum. Ω_0 is the present-day value of the density

parameter, while h describes the present-day value of the Hubble-parameter H_0 in units of $100 \text{ km s}^{-1} \text{ Mpc}^{-1}$.

In general, σ_8 increases with time, so it is an indication of time. For scenarios with $\Omega_0 = 1.0$, σ_8 evolves linearly with the expansion factor (e.g., Padmanabhan 1993) because the shape of the power spectrum is constant in time. In such a scenario the particle distribution at an epoch before the present time is identical to that at the present time in a scenario with a correspondingly smaller value of σ_8 . Consequently, the values of σ_8 given for the five $\Omega_0 = 1.0$ scenarios, are the maximum values of σ_8 that one can probe. The σ_8 values in Table 1 are roughly in agreement with the findings of Eke, Cole & Frenk (1996). These authors derived values for σ_8 equal to 0.50 ± 0.04 for $\Omega_0 = 1.0$ scenarios, 0.55 ± 0.04 for $\Omega_0 = 0.8$, and 1.03 ± 0.08 for $\Omega_0 = 0.2$ scenarios, by comparing their N-body simulations with the observed number density of clusters as a function of X-ray temperature. The LCDMa scenario has a normalization similar to the COBE-normalization, $\sigma_8 = 0.46$ (Sugiyama 1995).

For the scenarios with $\Omega_0 < 1.0$, the shape of the power spectrum does change with time and therefore the simple rescaling of the time coordinate in the $\Omega_0 = 1.0$ scenarios is impossible. In these scenarios the particle distribution at an epoch before the present time is identical to that at the present time in a scenario with a smaller value of σ_8 as well as larger values of Ω and the spectral parameter Γ . The latter was introduced by Efstathiou, Bond & White (1992) and measures the spectral shape. For CDM scenarios it is equal to Ωh . Scenarios with a larger value of Γ contain less power on large scales and slightly more power on small scales. For example, for the LCDMa and LCDMb scenario, the range in Γ is 0.10–0.27, for the LCDMc scenario 0.20–0.53, and for the LCDMd scenario 0.40–0.47, for expansion factors between 1.00 and 0.22.

n is the index of the primordial spectrum, with the canonical value of 1.0 corresponding to the Harrison–Zeldovich spectrum. The TCDM scenario has $n = 0.8$, i.e., its spectrum is slightly tilted and has somewhat more power on larger scales than standard CDM.

The LCDMd scenario is included to investigate the difference between a scenario with a value of Ω_0 less than but close to 1.0 and a scenario with $\Omega_0 = 1.0$. Because of the different dynamics between flat and open scenarios, the fact that Ω_0 is smaller than 1.0 may be more important for the cluster properties than how much Ω_0 is exactly below 1.0. As most studies for $\Omega_0 < 1.0$ so far usually adopt a 'very low' value for Ω_0 , i.e., ≈ 0.3 , this has never been checked thoroughly.

The implied present age of the Universe in each of the scenarios is given in column 7 of Table 1.

The expansion factor a_{exp} for which the particle positions and velocities are stored are almost always $a_{\text{exp}} = (0.22, 0.33, 0.44, 0.55, 0.66, 0.79, 0.89, 1.00)$, except for the SCDM and k^{-2} scenarios. For the SCDM scenario we have stored $a_{\text{exp}} = (0.25, 0.33, 0.41, 0.49, 0.59, 0.67, 0.75, 0.84, 0.90, 1.00)$ and for the k^{-2} scenario $a_{\text{exp}} = (0.16, 0.24, 0.31, 0.39, 0.47, 0.56, 0.64, 0.71, 0.86, 1.00)$. The redshift corresponding to a given expansion factor follows from $z = a_{\text{exp}}^{-1} - 1$.

2.2 Defining clusters

2.2.1 Group finding algorithm

The algorithm that we used to define groups is the "friends-of-friends" algorithm. It is described in, e.g., Davis *et al.* (1985). This algorithm links all particle pairs that are separated by less than a fraction p of the mean interparticle distance. Each subset of linked particles is then defined as a group. The algorithm finds groups that have an overdensity p^{-3} with respect to the mean background density. Since the overdensity $\delta\rho/\rho$ within the virial radius of a cluster is ≈ 180 (e.g., Padmanabhan 1993), typical values for p should be about 0.15–0.20. We adopt $p = 0.20$. The algorithm has the advantage that it produces a unique catalog of groups for any p , and that it does not make a priori assumptions about the shape of the groups.

Only groups containing at least 100 particles are included in the cluster list. This lower limit is adopted since fewer particles may result in a large increase in shot noise in the measurements. In the simulations 100 particles represent a mass of $2.22 \times 10^{14} h^{-1} \Omega_0 M_\odot$. This mass can be compared to the mass within the virialized part of clusters, which is about $5 \times 10^{14} h^{-1} M_\odot$.

2.2.2 Cluster definition

For the study of intrinsic properties of the model clusters, all groups with a mass larger than $2.22 \times 10^{14} h^{-1} M_\odot$ will be considered 'clusters' from now on. These clusters form our *mass-limited* cluster catalogue. This mass limit is similar to the mean cluster mass of $3 \times 10^{14} h^{-1} M_\odot$ that is expected for an isothermal model with a velocity dispersion of 700 km s^{-1} (Peebles 1993). Each cluster then contains at least $100/\Omega_0$ particles. This difference in mass resolution between $\Omega_0 = 1.0$ and $\Omega_0 = 0.2$ may influence the analyses. In Paper II we will address the problem of mass resolution more thoroughly by explicitly undersampling the clusters. We conclude there that this undersampling does not have any significant influence on the cluster properties.

The observed number density of rich ($R \geq 1$) Abell clusters is $8.6 \times 10^{-6} h^3 \text{ Mpc}^{-3}$ (e.g., Mazure *et al.* 1996). Thus, one expects about 144 rich clusters in our simulation volume. This number of 144 will be used when comparing the observed properties of the model clusters to real observations (Paper II). As in some of the scenarios the number of clusters with a mass above the limit is far less than 144, we have chosen to define for each scenario a *number-selected* cluster catalogue as well, consisting of the 144 most massive clusters. However, the mass ranges of those catalogues can be quite different. For example, in the LCDMb scenario the mass of the least massive cluster in the number-selected catalogues is $1.5 \times 10^{14} h^{-1} M_\odot$ while for the HDM scenario it is $7.7 \times 10^{14} h^{-1} M_\odot$. The mass of the most massive cluster ranges from $5.8 \times 10^{14} h^{-1} M_\odot$ to $2.0 \times 10^{15} h^{-1} M_\odot$.

For both definitions of the cluster sample, Figure 1 shows the percentage of all particles that is in clusters. This gives an idea of the importance of such clusters in the simulations. For the mass-limited samples, two scenarios clearly stand out, viz. the hCDM and HDM scenarios (lefthand panel). The reason for this is the large value of σ_8 for these scenarios (i.e., $\sigma_8 = 1.00$, see Table 1). At an expansion fac-

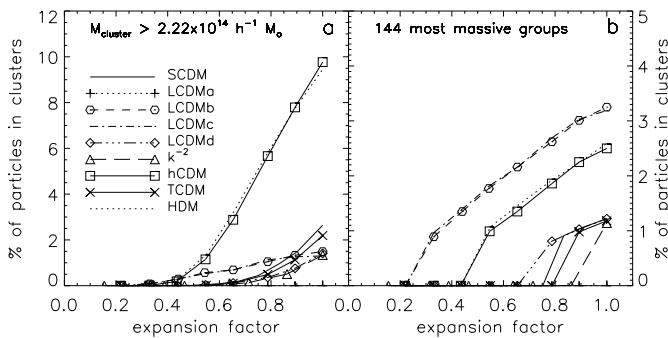


Figure 1. Percentage of particles in clusters. **a:** Clusters are defined as those groups which have a mass of at least $2.22 \times 10^{14} h^{-1} M_\odot$. **b:** Clusters are defined as the 144 most massive groups.

tor $a_{\text{exp}} \approx 0.65$, where both scenarios have $\sigma_8 \approx 0.65$, the fraction of particles in clusters is similar to that in other scenarios which also have $\sigma_8 \approx 0.65$. So, while studying the clusters that are defined in this way, one is treating a similar fraction of the total number of particles in each simulation cube.

The righthand panel of Figure 1 shows the percentage of particles in the 144 most massive groups. Again, the hCDM and HDM scenarios stand out, but now the two $\Omega_0 = 0.2$ scenarios LCDM_b and LCDM_c have an even larger fraction of the particles in clusters, almost three times as much as for the other scenarios. If one would rescale these scenarios to lower σ_8 by investigating the scenario at earlier times, the density parameter Ω and the spectral parameter Γ also change. So the fraction of particles involved shows a broader range than for the mass-limited samples. However, we use the number-selected sample only if the results of the mass-limited sample may be influenced by the limited number of clusters in the latter sample.

2.2.3 Cluster centres

To determine the cluster centre, two methods are used. The first one is the same as in de Theije, Katgert & van Kampen (1995). First, one calculates the centre of mass of all particles in the cluster. Then one defines an aperture of radius $1.0h^{-1}$ Mpc around this centre and calculates the new centre of all particles within this aperture. This procedure is repeated until the mass centre does not shift by more than $0.1h^{-1}$ Mpc.

In the second approach to define the cluster centre we find the particle which has the largest smoothed density of particles around it. This density is calculated by smoothing the particle distribution around each particle with a Gaussian distribution of dispersion R_s , which is equal to half the average nearest neighbour distance $[3/4\pi\langle n \rangle]^{1/3}$, where $\langle n \rangle$ is the mean number density of particles (see van Kampen 1995). This definition resembles the X-ray centre of a cluster, because the X-ray emission is proportional to the electron density squared of the intracluster gas.

We have checked that the cluster mass is the same for both definitions of cluster centre, and expect this to be true

for the other cluster properties as well. As the first method is much less time consuming, we use that method in what follows.

2.3 Galaxy identification

Different schemes have been used in the literature to identify galaxies in N-body simulations (e.g., White *et al.* 1987, Nolthenius, Klypin & Primack 1994). In most of the schemes one identifies galaxies as the highest peaks above a threshold given by some bias factor. Van Kampen (1995) described the formation and evolution of galaxies by replacing a group of particles that is roughly in virial equilibrium by a single soft particle with mass, position, velocity and softening corresponding to that group. His constrained random field single cluster simulation cubes were much smaller than the present ones and each particle had a mass of $3.5 \times 10^{10} h^{-1} M_\odot$. As the particles in our simulations have a mass of $2.22 \times 10^{12} \Omega_0 h^{-1} M_\odot$, already the mass of a galaxy, it is impossible to apply this algorithm here.

Instead, we assume the dark matter to be equally distributed as the luminous matter, i.e., galaxies and gas. Buote & Canizares (1996) concluded that, for their sample of 5 clusters, the shapes of the dark matter distribution, the mass distribution and galaxy isopleths are all consistent with each other. In addition, for the catalogue of model clusters of van Kampen (1995), the distributions of ellipticities for the galaxy particles on the one hand, and for all dark matter particles on the other hand are statistically the same.

From a sample of 41 clusters with measured velocity dispersions and X-ray temperatures, Lubin & Bahcall (1993) concluded that the velocity bias in clusters, $b_v \equiv \sigma_{\text{gal}}/\sigma_{\text{DM}} = 0.97 \pm 0.04$. So the velocity dispersion of the galaxies is almost identical to that of the dark matter. Also, van Kampen (1995) found no evidence for velocity bias in his catalogue of cluster models which contain a recipe for galaxy formation. In addition, several authors concluded that the spatial distribution of the galaxies, gas and the total mass are all very similar, with possibly a somewhat larger central concentration for the dark matter (e.g., Henry, Briel & Nulsen 1994, Smail *et al.* 1995, Tyson & Fischer 1995, Squires *et al.* 1996).

3 CLUSTER NUMBER DENSITIES

An important property of the cluster distribution as a whole is the number density of rich Abell clusters in the simulations. In the present paper we define the cluster sample to be all groups in the simulation that have a mass of at least $2.22 \times 10^{14} h^{-1} M_\odot$ (see Section 2.2.2), i.e., the mass-limited catalogue.

In Table 2 we give the number of clusters in each simulation, i.e., the number of groups which have a mass of at least $2.22 \times 10^{14} h^{-1} M_\odot$ within a clustercentric radius of $1.0h^{-1}$ Mpc at various times. For the SCDM scenario, these values are similar to the predicted number of clusters above this minimum mass as derived from the Press-Schechter formalism (Eke *et al.* 1996). The numbers in parentheses in Table 2 give the mean number of particles per cluster within $1.0h^{-1}$ Mpc, averaged over all clusters. This mean number

Table 2. Number of clusters with a mass within $r = 1.0h^{-1}$ Mpc of at least $2.22 \times 10^{14}h^{-1}M_\odot$, corresponding to $100/\Omega_0$ particles. The numbers in parentheses give the mean number of particles per cluster, averaged over all clusters.

scenario	expansion factor							
	0.22	0.33	0.44	0.55	0.66	0.79	0.89	1.00
LCDMa	0	0	0	0	0	0	0	0
LCDMb	1	5 (319)	17 (360)	30 (396)	29 (501)	39 (567)	44 (637)	46 (679)
LCDMc	1	5 (316)	17 (341)	28 (396)	32 (461)	42 (563)	41 (644)	41 (662)
LCDMd	0	0	0	6 (127)	18 (138)	51 (146)	100 (160)	181 (164)
hCDM	0	2 (108)	30 (130)	181 (134)	424 (143)	749 (159)	962 (170)	1166 (176)
TCDM	0	0	0	3 (108)	18 (131)	82 (126)	180 (132)	338 (136)
HDM	0	2 (121)	38 (129)	205 (139)	455 (151)	747 (163)	928 (175)	1062 (187)

scenario	expansion factor									
	0.25	0.33	0.41	0.49	0.59	0.67	0.75	0.84	0.90	1.00
SCDM	0	0	0	1 (106)	12 (128)	34 (122)	77 (124)	159 (127)	232 (134)	406 (136)

scenario	expansion factor									
	0.16	0.24	0.31	0.39	0.47	0.56	0.64	0.71	0.86	1.00
k^{-2}	0	0	0	0	0	1 (100)	8 (131)	23 (125)	72 (147)	189 (149)

of particles increases towards later times for all cosmological scenarios, illustrating the growth of the clusters.

In the LCDMa scenario, no clusters with $M \geq 2.22 \times 10^{14}h^{-1}M_\odot$ are formed for the assumed value $\sigma_8 = 0.46$ in the simulation. Therefore, we will not consider this scenario any further.

If one evaluates the *total* mass of the clusters, using the entire group as defined by the friends-of-friends algorithm, the results are qualitatively the same as when one uses the mass within $1.0h^{-1}$ Mpc.

4 INTRINSIC PROPERTIES OF CLUSTERS

The intrinsic properties of the model clusters are evaluated using both the mass-limited and the number-selected cluster catalogues. In the following analyses, all cluster particles that are within a clustercentric radius of $r = 1.0h^{-1}$ Mpc are considered, unless stated otherwise.

4.1 Masses

The first, most basic, property of the clusters that we will investigate is their mass M . Figure 2 shows the cumulative distribution $\rho(< M)$ of particle mass for all clusters in the mass-limited sample. For the $\Omega_0 = 1.0$ scenarios, different values of σ_8 are plotted. In these cases, σ_8 is highest for the upper curves and decreases downward. In the upper righthand panel, the low- Ω_0 scenarios are shown. For the $\Omega_0 = 1.0$ scenarios, the cluster mass increases with σ_8 , or, equivalently, with time. If one were to extrapolate this to $\sigma_8 = 0.9$, the value adopted for the LCDMb and LCDMc scenarios, the clusters in the $\Omega_0 = 1.0$ scenarios have a much larger mass than those in these two low- Ω_0 scenarios for the same value of σ_8 . Even in the LCDMd scenario with

$\Omega_0 = 0.8$, the cluster mass is significantly smaller than in the SCDM scenario with $\sigma_8 = 0.61$.

A comparison of the distributions for the LCDMb and LCDMc scenarios is a check of the calculations, as these scenarios are exactly the same apart from the value of the Hubble parameter h . As the masses here are expressed in units of $10^{14}h^{-1}M_\odot$, there should be no difference at all between these two scenarios for their cluster masses. Indeed, we find very good agreement.

Among the different scenarios, the particle mass of clusters may be quite different. The low- Ω_0 scenarios have a most massive cluster of about $6 \times 10^{14}h^{-1}M_\odot$. The SCDM, k^{-2} and TCDM scenarios contain masses up to $\approx 8 \times 10^{14}h^{-1}M_\odot$. The hCDM and HDM scenarios contain clusters of even larger mass, $18 \times 10^{14}h^{-1}M_\odot$. This is due to the high value of σ_8 , viz. $\sigma_8 = 1.00$, in these latter two scenarios.

For all $\Omega_0 = 1.0$ scenarios the slope of $\rho(> M)$ is clearly flatter at later times, showing that the relative number of high-mass clusters increases at later times. The change in the median value of the cluster particle mass, however, is not very large. This is clear from Table 3, which shows the median value of the cluster particle mass for different values of a_{exp} . Only for the hCDM and HDM scenarios is there an increase in the median value towards later times. For all other scenarios the increase is not significant or not monotonic.

The median value of the cluster particle mass in the low- Ω_0 scenarios changes less rapidly with time. To illustrate the change of cluster mass in these open scenarios, we show in Figure 3 the change of the particle mass distribution of the low- Ω_0 scenarios LCDMc and LCDMd with time. For the LCDMc scenario, the cluster population does not evolve strongly for redshifts $z \leq 0.50$. I.e., the total number of

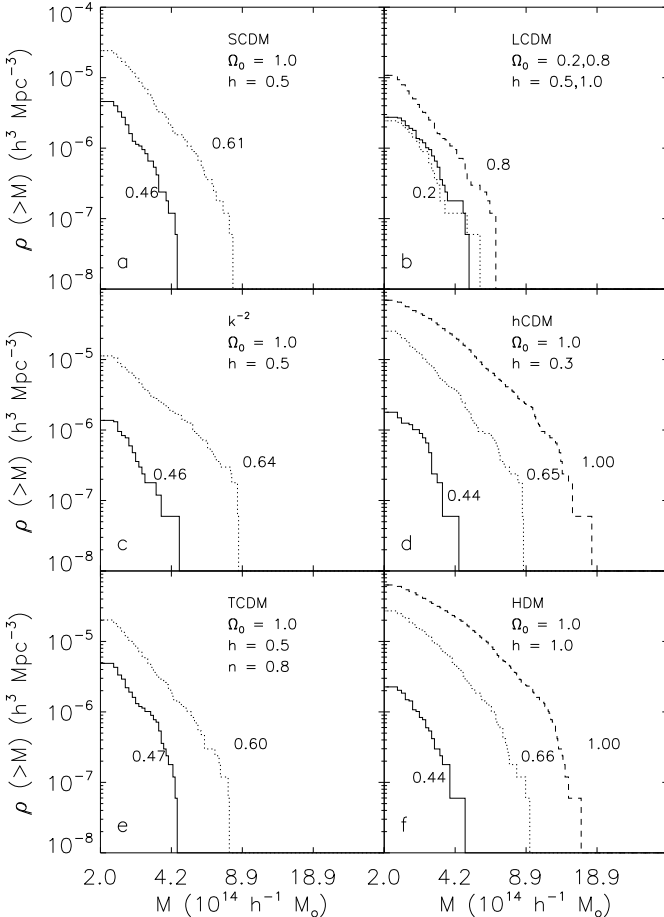


Figure 2. Cumulative distribution of cluster particle masses for all clusters having a particle mass of at least $2.22 \times 10^{14} h^{-1} M_\odot$. **a:** SCDM with $\sigma_8 = 0.46$ (solid line) and $\sigma_8 = 0.61$ (dotted line). **b:** LCDMb (solid line), LCDMc (dotted line) and LCDMd (dashed line). **c:** k^{-2} with $\sigma_8 = 0.46$ (solid line) and $\sigma_8 = 0.64$ (dotted line). **d:** hCDM with $\sigma_8 = 0.44$ (solid line), $\sigma_8 = 0.65$ (dotted line) and $\sigma_8 = 1.00$ (dashed line). **e:** TCDM with $\sigma_8 = 0.47$ (solid line) and $\sigma_8 = 0.60$ (dotted line). **f:** HDM with $\sigma_8 = 0.44$ (solid line), $\sigma_8 = 0.66$ (dotted line) and $\sigma_8 = 1.00$ (dashed line).

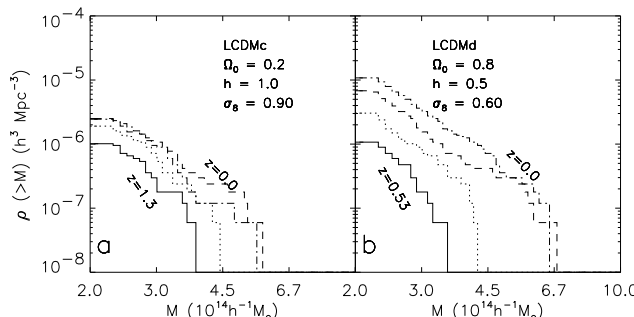


Figure 3. Time evolution of the cumulative distribution of cluster particle mass. Only clusters with a mass of at least $2.22 \times 10^{14} h^{-1} M_\odot$ are considered. **a:** LCDMc scenario. The curves correspond to redshifts $z = 1.3$ (solid line), 0.53 (dotted line), 0.27 (dashed line), and 0.0 (dot-dashed line). **b:** LCDMd scenario. The curves correspond to redshifts $z = 0.53$ (solid line), 0.27 (dotted line), 0.12 (dashed line), and 0.0 (dot-dashed line).

Table 3. Evolution parameters of the mass of all clusters having a mass of at least $2.22 \times 10^{14} h^{-1} M_\odot$. The values in this table denote the median values of the cluster particle mass M (in units of $10^{14} h^{-1} M_\odot$). The information is listed only for expansion factors at which there are at least 10 clusters.

median value of cluster particle mass (in $10^{14} h^{-1} M_\odot$)

scenario	expansion factor						
	0.44	0.55	0.66	0.79	0.89	1.00	
LCDMb				2.9	2.9	3.0	2.9
LCDMc					2.8	3.1	2.8
LCDMd				2.6	2.5	2.6	2.7
hCDM	2.9	2.7	2.8	3.1	3.2	3.3	
TCDM			2.7	2.6	2.7	2.7	
HDM	2.7	2.8	3.0	3.2	3.3	3.5	

scenario	expansion factor					
	0.59	0.67	0.75	0.84	0.90	1.00
SCDM	2.8	2.7	2.6	2.6	2.8	2.8

scenario	expansion factor					
	0.47	0.56	0.64	0.71	0.86	1.00
k^{-2}				2.7	3.0	2.8

clusters is more or less constant and only a few high-mass clusters increase their mass even further. This result is quantitatively consistent with that of, e.g., Eke *et al.* (1996). In the LCDMd scenario, the situation is quite different. Here the number of clusters increases up to the present time and the maximum mass increases somewhat faster than in the LCDMc scenario. So there is a clear difference in the time-evolution of cluster mass with Ω_0 , even between scenarios with $\Omega_0 < 1.0$. Alternatively, the different curves in Figure 3 can also be viewed as corresponding to scenarios with a different value of Γ (see Section 2.1). In that case, Γ is lowest for the upper curves. Scenarios with a larger value of Γ then seem to have less clusters above a certain mass, but this result is solely due to the different values of σ_8 that correspond to the different curves.

If one uses the average mass estimator (Heisler, Tremaine & Bahcall 1985)

$$M_{\text{ave}} = \frac{5.6}{GN(N-1)} \sum_{i < j} (v_{zi} - v_{zj})^2 R_{ij}, \quad (1)$$

where G is the gravitational constant, N the total number of particles, v_{zi} is the velocity of galaxy i w.r.t. the cluster center, and R_{ij} is the distance between galaxies i and j , then the cumulative distributions of cluster masses look very similar to the distributions of cluster particle mass. The average mass estimator, however, overpredicts the cluster particle mass by about 40% in all scenarios. The projected mass estimator overpredicts the cluster particle mass even more than the average mass estimator. These results are quantitatively similar to those of van Kampen (1995), who used N-body simulations of single clusters in an $\Omega_0 = 1.0$ CDM Universe to test the mass estimators. He found that

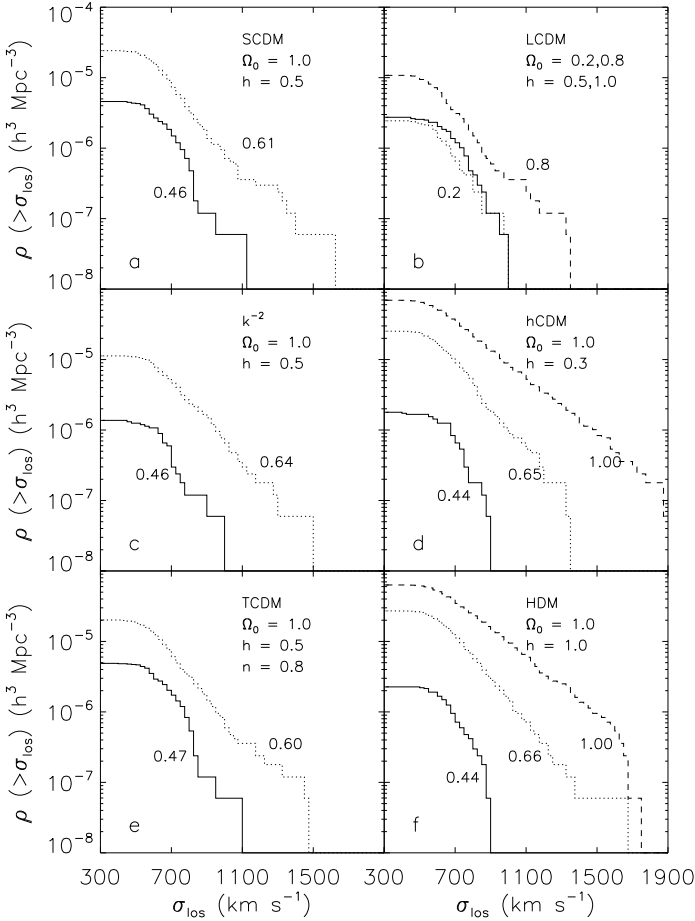


Figure 4. Cumulative distribution of line-of-sight velocity dispersion for clusters in the different cosmological scenarios. Only clusters with a mass of at least $2.22 \times 10^{14} h^{-1} M_\odot$ are considered. The different panels and curves have the same meaning as in Figure 2.

the average mass estimator overpredicts the cluster mass by about 40%, if evaluated within about $1.0h^{-1}$ Mpc, and that the projected mass estimator overpredicts the cluster mass by about 60%.

To investigate how the mass increases with cluster-centric radius, we determine the mass of the clusters within an Abell radius, $1.5h^{-1}$ Mpc. Using the particle mass for this, the mass within the Abell radius is about 25–35% larger than that within $1.0h^{-1}$ Mpc. This is more or less what is expected for a spherical cluster whose density profile follows a modified Hubble law $\rho(r) = \rho(0)/[1 + (r/r_c)^2]^{3/2}$ with a core radius of $r_c = 0.25h^{-1}$ Mpc (e.g., Sarazin 1986).

If one uses the number-selected cluster samples, the cumulative distributions of cluster mass would be very similar to the curves in Figure 2 of the mass-limited samples. The distributions of cluster average mass change in the same way as those over cluster particle mass, but the transition between $\rho(> M) \leq 8.6 \times 10^{-6} h^3 \text{ Mpc}^{-3}$ and $\rho(> M) \geq 8.6 \times 10^{-6} h^3 \text{ Mpc}^{-3}$ is now rather smooth because of the scatter in the relation between a cluster's particle mass and average mass.

Table 4. Evolution parameters of the line-of-sight velocity dispersion of all clusters having a mass of at least $2.22 \times 10^{14} h^{-1} M_\odot$. The values in this table denote the median values of the line-of-sight velocity dispersion σ_{los} (in km s^{-1}). The information is listed only for expansion factors at which there are at least 10 clusters.

scenario	median value of cluster line-of-sight velocity dispersion					
	expansion factor					
	0.44	0.55	0.66	0.79	0.89	1.00
LCDMb			652	665	672	683
LCDMc				654	657	635
LCDMd			625	661	646	619
hCDM	670	638	642	661	679	690
TCDM				634	654	628
HDM	663	649	669	686	702	719

scenario	expansion factor					
	0.59	0.67	0.75	0.84	0.90	1.00
SCDM	568	650	645	632	638	637

scenario	expansion factor					
	0.47	0.56	0.64	0.71	0.86	1.00
k^{-2}				637	679	665

4.2 Line-of-sight velocity dispersions

The next property of clusters that we consider is their line-of-sight velocity dispersion σ_{los} , which describes the dynamical state of the cluster, as it is influenced by merging events, substructure and the shape of the galaxy orbits.

Crone & Geller (1995) studied the evolution of the cluster velocity dispersion using large-scale N-body simulations. They concluded that σ_{los} can be significantly influenced by merger activity and therefore does not simply reflect the cluster mass (they found a scatter of about 5–10% in σ_{los} for clusters of the same mass). Furthermore, they detected some change in σ_{los} with time. The slope of the cumulative distribution of the number density of clusters with a velocity dispersion larger than σ_{los} , $\rho(> \sigma_{\text{los}})$, flattens with time, so that at later times more clusters are found with large σ_{los} . The change with time is most evident for scenarios with a high value of Ω_0 .

The velocity dispersion for the clusters in our N-body simulations is calculated using the robust biweight estimator of Beers, Flynn & Gebhardt (1990), yet the velocity dispersions are essentially the same with the ordinary definition. The cumulative distributions of line-of-sight velocity dispersion found in our simulations are plotted in Figure 4. As before, these distributions include all clusters which have a mass of at least $2.22 \times 10^{14} h^{-1} M_\odot$. The different panels and curves have the same meaning as in Figure 2, i.e., for the $\Omega_0 = 1.0$ scenarios the higher curves correspond to larger values of σ_8 .

For the $\Omega_0 = 1.0$ scenarios, our results are consistent with those of Jing & Fang (1994) and Crone & Geller (1995). That is, the curves for lower σ_8 , or, alternatively, higher z

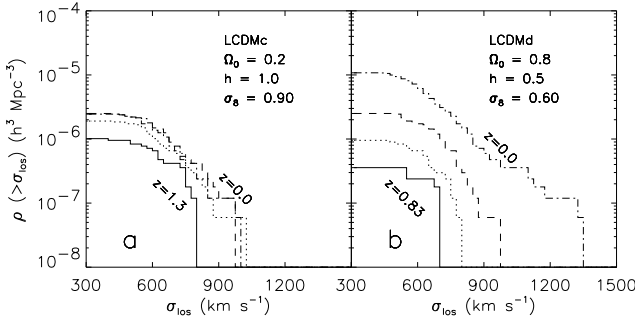


Figure 5. Time evolution of the cumulative distribution of cluster velocity dispersions. Only clusters with a mass of at least $2.22 \times 10^{14} h^{-1} M_{\odot}$ are considered. **a:** LCDMc scenario. The curves correspond to redshifts $z = 1.3$ (solid line), 0.53 (dotted line), 0.27 (dashed line), and 0.0 (dot-dashed line). **b:** LCDMd scenario. The curves correspond to redshifts $z = 0.83$ (solid line), 0.53 (dotted line), 0.27 (dashed line), and 0.0 (dot-dashed line).

(see Section 2.1), are steeper than the $z = 0$ curves (the upper ones). Clearly, the evolution of velocity dispersions is not self-similar: the curve shifts towards higher σ_{los} , but at the same time it flattens. At the present epoch, clusters with a high σ_{los} are relatively more abundant than clusters with a low value of σ_{los} . These changes in time are analogous to that for the mass of the clusters (see the previous section). Table 4 lists the median values of σ_{los} for the cluster sample at all time steps and for all scenarios for which there is a significant number of clusters present that satisfy the minimum mass criterion. The scenarios with a low σ_8 have relatively smaller values of σ_{los} . This is because less matter has collapsed on cluster scales. On the other hand, clusters that are not in the sample at early times, because their mass is too low, can enter the sample at later times and populate the low- σ_{los} part of the distribution. The combination of both facts results in an apparent upward shift of the whole distribution. Only the hCDM and HDM scenarios show a significant increase in the median value of σ_{los} with time. For both scenarios we already concluded that the median values of the cluster particle mass increase with time (see Section 4.1).

As an example of the evolution of the velocity dispersions in low- Ω_0 scenarios, we show $\rho(> \sigma_{\text{los}})$ for the LCDMc and LCDMd scenarios in Figure 5. For the LCDMc scenario, $\rho(> \sigma_{\text{los}})$ hardly changes for $z \leq 0.50$. The number of high- σ_{los} clusters remains constant, as does the maximum value of σ_{los} . This is consistent with results of Jing & Fang (1994) who found no evolution in $\rho(> \sigma_{\text{los}})$ for $z \leq 0.5$ for their sample of clusters with mass larger than $1.7 \times 10^{13} M_{\odot}$. Note that these authors used $\Omega_0 = 0.3$. In addition, σ_{los} does not exceed 1000 km s^{-1} , in contrast to most of the $\Omega_0 = 1.0$ scenarios. For the LCDMd scenario the situation is quite different. The number of clusters rises until the present time. The median value of σ_{los} , however, is fairly constant. For the different values of Ω_0 , $\rho(> \sigma_{\text{los}})$ changes with time in a similar manner as $\rho(> M)$ (see Section 4.1).

For the hCDM and HDM scenarios the fractional change in mass is, in general, about twice as large as for the velocity dispersion (Tables 3 and 4), consistent with the virial theorem estimates. This evolutionary difference be-

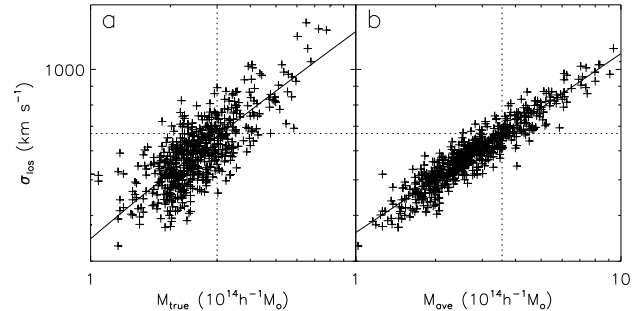


Figure 6. Scatter plot of the cluster line-of-sight velocity dispersion σ_{los} versus its mass for clusters in the SCDM scenario. The solid line shows the relation $\sigma \propto \sqrt{M_{\text{ave}}}$. The horizontal and vertical dotted lines indicate the values of σ_{los} and M , respectively, of the 144-th most massive group, in terms of the particle mass. **a:** σ_{los} versus cluster particle mass. **b:** σ_{los} versus cluster average mass estimator M_{ave} .

tween mass and velocity dispersion is also consistent with the findings of Crone & Geller (1995), who found that the velocity dispersion evolves less rapidly than the mass of a cluster. They attributed this to two processes: first, for a specific mass range, the velocity dispersion decreases with time due to relaxation. Secondly, mergers will make the distribution of σ_{los} more irregular than that over mass. That is, the scatter in the $\sigma_{\text{los}} - M$ -relation due to mergers and accretions introduces random fluctuations in $\rho(> \sigma_{\text{los}})$.

To check how large the scatter between σ_{los} and M is, we show in the lefthand panel of Figure 6 the line-of-sight velocity dispersion versus particle mass for all clusters in the SCDM scenario for $\sigma_8 = 0.61$. The solid line shows, for comparison, the best-fitting relation $\sigma_{\text{los}} \propto \sqrt{M}$, as expected for systems in virial equilibrium. The *r.m.s.* scatter about this relation is about 14%, somewhat larger than the 5–10% that Crone & Geller (1995) found. These results are similar for all scenarios. For comparison, the righthand panel of Figure 6 shows the same scatter plot but using the average mass estimator. The scatter about the linear relation $\sigma_{\text{los}} \propto \sqrt{M_{\text{ave}}}$ is smaller than if using the cluster particle mass, namely 7%. So although the average mass estimator overestimates the cluster particle mass by about 40% (see Section 4.1), it correlates better with the cluster line-of-sight velocity dispersion than does the cluster particle mass. This is because both the velocity dispersion and the average mass estimator explicitly use the particle velocities whereas the particle mass does not contain this information.

The horizontal and vertical dotted lines in Figure 6 indicate the values of σ_{los} and M , respectively, of the 144-th most massive cluster, in terms of the particle mass. These values will be called σ_{144} and M_{144} from here on. This comparison gives an idea of how complete, in terms of mass, a sample of clusters will be that is selected on the basis of their velocity dispersion. This is the case, e.g., for the ENACS-survey (Katgert *et al.* 1996), that is claimed to be complete for $\sigma_{\text{los}} \geq 800 \text{ km s}^{-1}$. Remember that we expect 144 clusters in a simulation box of $(256 h^{-1} \text{ Mpc})^3$ on the basis of the cluster number density of the ENACS-survey. When one uses the cluster particle mass, the fraction of clusters with $\sigma_{\text{los}} \geq \sigma_{144}$ that also have $M \geq M_{144}$ ranges from 64%

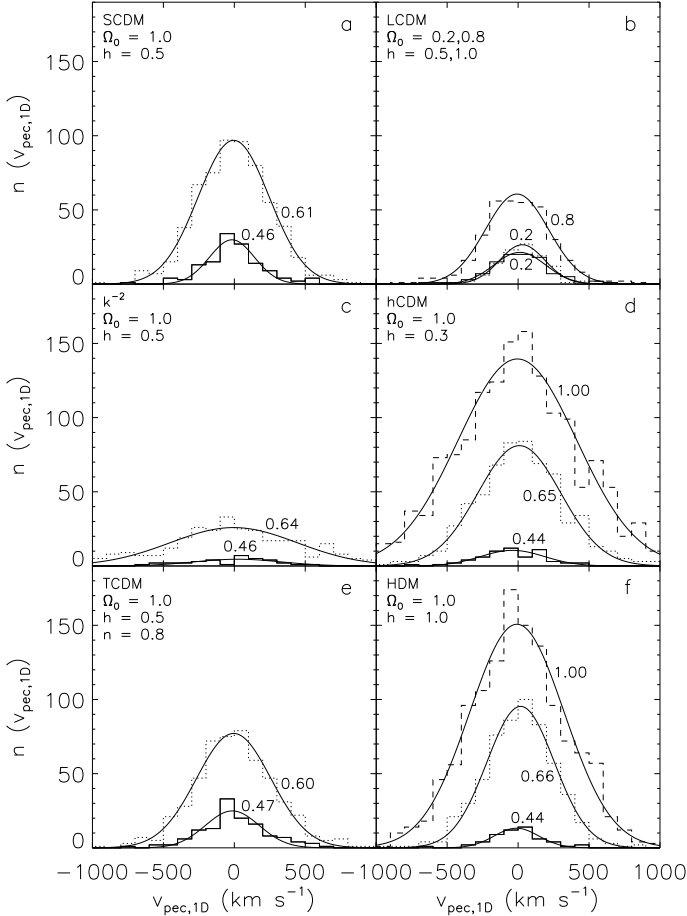


Figure 7. Distributions of 1-D peculiar velocities of clusters in the different cosmological scenarios. The different panels and curves have the same meaning as in Figure 2. The solid lines show the best-fitting Gaussian distributions. The parameters of these are listed in Table 4.

(SCDM) to 78% (for the k^{-2} scenario). These numbers are comparable to the 66% of clusters of richness class $R \geq 1$ in the Abell catalogue that also has the required intrinsic richness (van Haarlem, Frenk & White 1997).

To check if the velocity dispersion changes with cluster-centric radius, we calculate the value of σ_{los} within a cluster-centric radius $r = 1.5h^{-1}$ Mpc. The velocity dispersions within the canonical Abell radius of $1.5h^{-1}$ Mpc are, on average, 5% smaller than those within $1.0h^{-1}$ Mpc. The exact numbers range from 2% to 7% and depend on the scenario and on the value of σ_8 .

For the number-selected cluster samples, the curves of $\rho(>\sigma_{\text{los}})$ would be very similar to those of the mass-limited samples. For those scenarios that have at least 144 clusters in the mass-limited samples, the curve for the number-selected sample is equal to that of the mass-limited sample for $\rho(>\sigma_{\text{los}}) \leq 8.6 \times 10^{-6}h^3 \text{ Mpc}^{-3}$, and flattens off smoothly to this constant value for lower σ_{los} . The transition is smooth because of the scatter in the $\sigma_{\text{los}} - M$ -relation (see Figure 6). For scenarios that have less than 144 clusters in the mass-limited sample, the curve for the number-selected sample has the same slope for high σ_{los} and extends to lower σ_{los} until it flattens off towards $\rho(>\sigma_{\text{los}}) = 8.6 \times 10^{-6}h^3 \text{ Mpc}^{-3}$.

Table 5. Parameter values of the Gaussian fits to the distributions of cluster peculiar velocities. The first two columns specify the scenario. The third and fourth columns describe the best-fitting Gaussian distribution, $f(v_{\text{pec},1D}) \propto \exp(-(v_{\text{pec},1D} - v_{\text{pec},1D,0})^2/2\sigma_{\text{pec},1D}^2)$. The fifth column gives the dispersion for the distribution of 3-D cluster peculiar velocities. Column 6 gives the predictions of BBKS. See text for more details.

scenario	σ_8	$v_{\text{pec},1D,0}$ (km s $^{-1}$)	$\sigma_{\text{pec},1D}$ (km s $^{-1}$)	$\sigma_{\text{pec},3D}$ (km s $^{-1}$)	σ_{BBKS} (km s $^{-1}$)
SCDM	0.46	-16.7	159	201	218
SCDM	0.61	-4.4	251	267	289
LCDMb	0.90	12.0	182	216	281
LCDMc	0.90	29.4	160	181	212
LCDMd	0.60	-7.3	223	247	263
k^{-2}	0.46	22.9	308	309	—
k^{-2}	0.64	-4.6	447	508	—
hCDM	0.44	-39.3	225	242	187
hCDM	0.65	8.9	292	318	276
hCDM	1.00	-4.6	419	438	424
TCDM	0.47	-14.0	190	230	234
TCDM	0.60	-4.2	262	280	299
HDM	0.44	-11.1	157	184	135
HDM	0.66	-18.0	238	254	202
HDM	1.00	-8.0	333	341	307

4.3 Peculiar velocities

The next property of galaxy clusters that we consider is the distribution of cluster peculiar velocities, i.e., the velocity of a cluster with respect to the Hubble-flow. This peculiar velocity is calculated using the robust biweight estimator of Beers *et al.* (1990).

Figure 7 shows the differential distributions of 1-D peculiar velocity $v_{\text{pec},1D}$ of all clusters in the mass-limited sample in all scenarios. Also shown are the best-fitting Gaussian distributions. Such Gaussian distributions are expected for Gaussian random fields (eq. 4.23 of Bardeen *et al.* 1986, hereafter BBKS). In general, the Gaussian distributions provide good fits. The fitting parameters are given in columns 3 and 4 of Table 5. The mean value for the best-fitting Gaussian distributions always differ from zero by less than 40 km s $^{-1}$. This is expected because there is neither any preferred direction in the simulation box nor any systematic flows on the scale of the simulation box. The dispersion of the fitted Gaussian distributions increases with σ_8 , or equivalently cosmic time, for the $\Omega_0 = 1.0$ scenarios.

For a specific value of σ_8 , the dispersion of the fitted Gaussian distribution is smaller for the $\Omega_0 < 1.0$ scenarios than for the $\Omega_0 = 1.0$ scenarios, consistent with earlier findings of, e.g., Bahcall, Gramann & Cen (1994). Again, this is because in the open scenarios less matter has collapsed on large scales and the total gravitational force acting on a cluster is smaller.

In order to check if the cluster peculiar velocities are

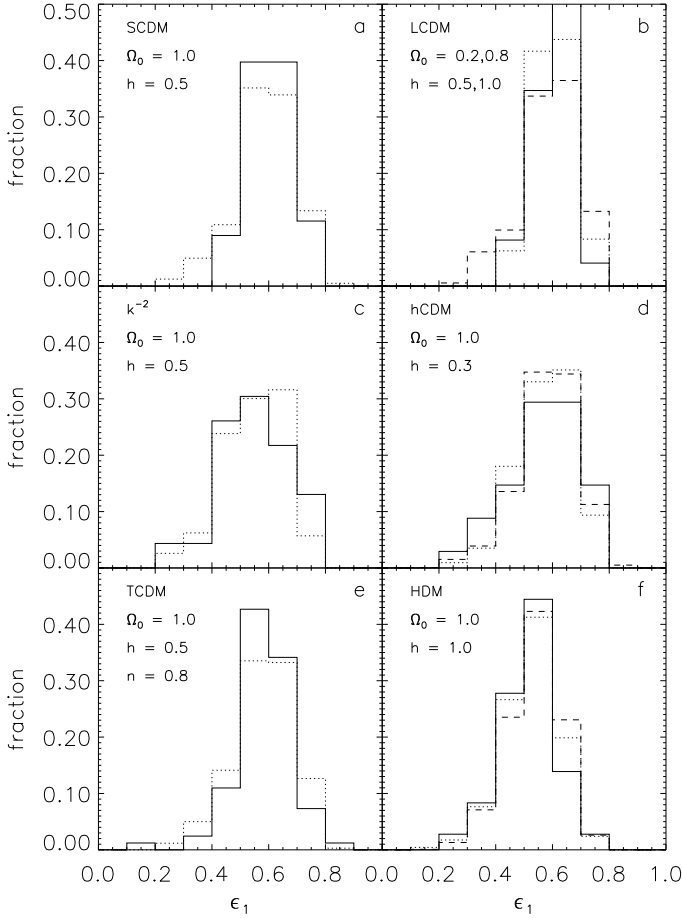


Figure 8. Distribution of intrinsic cluster ellipticities ϵ_1 for different cosmological scenarios. $\epsilon_1 = 0.0$ means that the cluster is spherical, $\epsilon_1 = 1.0$ means that the particle distribution of the cluster is a disk. Only clusters with a mass of at least $2.22 \times 10^{14} h^{-1} M_\odot$ are taken into account. The different panels and curves have the same meaning as in Figure 2.

distributed isotropically, we investigate the distribution of 3-D peculiar velocities, $v_{\text{pec},3\text{D}}$. If the cluster peculiar velocities are distributed isotropically, the 3-D peculiar velocity vectors should have a random orientation. We check this by determining the distributions of spherical angles ϕ and $\cos(\theta)$ of the velocity vector. These distributions are indeed consistent with uniform distributions for all scenarios. Column 5 of Table 5 lists the dispersions $\sigma_{3\text{D}}$ of the Maxwellian fits $f(v_{\text{pec},3\text{D}}) \propto v_{\text{pec},3\text{D}}^2 \exp(-(v_{\text{pec},3\text{D}} - v_{\text{pec},3\text{D},0})^2/2\sigma_{\text{pec},3\text{D}}^2)$ to the distributions of 3-D cluster peculiar velocity. Column 6 gives the expected dispersions of these distributions using linear theory (BBKS). For the k^{-2} scenario, the values of BBKS cannot be obtained because of physical reasons. The values of $\sigma_{3\text{D}}$ for the model clusters are comparable to the expected values of BBKS. However, for the $\Omega_0 = 0.2$ scenarios the values for the model clusters are systematically lower than expected. For the hCDM and HDM scenarios they are slightly higher, especially for lower values of σ_8 . Apparently, the hCDM and HDM scenarios have grown non-linear on the larger scales.

4.4 Shapes

De Theije *et al.* (1995) used the results of N-body simulations of van Kampen (1994) to study how the shapes of clusters may depend on cosmological scenario. They found that in a low- Ω_0 CDM Universe, clusters are, on average, more nearly spherical than the *same* clusters in an $\Omega_0 = 1.0$ Universe. This conclusion was also reached by Mohr *et al.* (1995) who determined cluster morphologies from SPH-simulations. These calculations showed that the X-ray shapes of clusters are less flattened spherical for low values of Ω_0 than in an Einstein-de Sitter Universe. Wilson, Cole & Frenk (1996) also concluded that clusters in an $\Omega_0 = 0.2$ Universe are more nearly spherical and centrally concentrated than clusters in an $\Omega_0 = 1.0$ Universe. On the basis of this result they constructed a new lensing statistic that is very sensitive to the value of Ω_0 and almost independent of the value of the cosmological constant Λ .

4.4.1 Distribution of intrinsic shape

To investigate which cosmological parameters influence the shape of a cluster, we determine the shape of the clusters for all scenarios. The present simulations are unconstrained, unlike the simulations of van Kampen & Katgert (1997), and we cannot compare *individual* clusters in different scenarios. Instead, we have to compare the *entire distribution* of cluster shapes. We describe the shape by two ellipticities which are obtained using the tensor of inertia, which was shown to yield reliable cluster ellipticities (de Theije *et al.* 1995). The tensor of inertia is defined as

$$I_{ij} = \sum_k x_{ik} x_{jk} / r_k^2 \quad (i, j = 1, 2), \quad (2)$$

where the sum is over all particles in the cluster, x_{ik} ($i = 1, 2$) are the coordinates of particle k with respect to the cluster centre and r_k is the distance of that particle to the cluster centre. The intrinsic cluster ellipticities are then given by

$$\epsilon_1 = 1 - \frac{c}{a}, \quad \epsilon_2 = 1 - \frac{b}{a}, \quad (3)$$

where $a \geq b \geq c$ are the eigenvalues of the tensor of inertia I (Eq. 2). The triaxiality parameter T was introduced by Franx, Illingworth & de Zeeuw (1990):

$$T = \frac{\epsilon_2(2 - \epsilon_2)}{\epsilon_1(2 - \epsilon_1)} = \frac{a^2 - b^2}{a^2 - c^2}. \quad (4)$$

A value of $T = 1.0$ indicates that a cluster is prolate while a value of $T = 0.0$ represents an oblate cluster. Values between 0.0 and 1.0 describe triaxial clusters for which a , b and c all have different values.

Figure 8 shows the distributions of ϵ_1 . There are no obvious differences among the different scenarios. For all scenarios there is a very small number of spherical clusters ($\epsilon_1 = 0$) and the largest cluster ellipticity is about 0.8. However, the Kolmogorov-Smirnov (KS from here on) test (e.g., Press *et al.* 1989), shows some differences between different scenarios. The k^{-2} scenario with $\sigma_8 = 0.64$ and the HDM scenario are significantly different from the SCDM, LCDM_b, LCDM_c, LCDM_d, hCDM and TCDM scenarios. Clusters in the k^{-2} and HDM scenarios have somewhat smaller ellipticities than those in the other scenarios. The distributions for

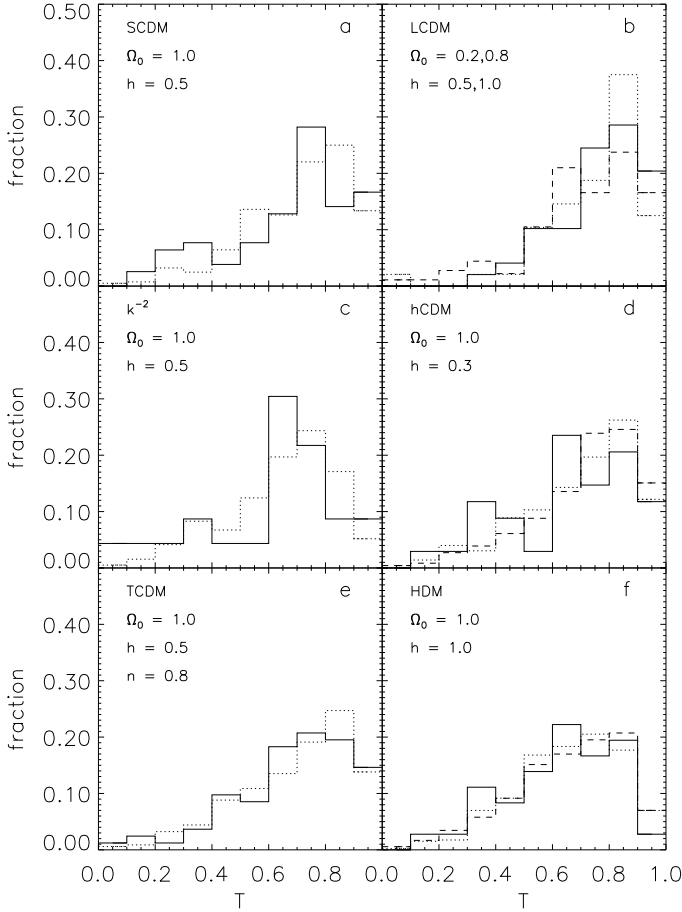


Figure 9. Distribution of triaxiality parameter T for clusters in the different scenarios. Only the clusters that have a mass of at least $2.22 \times 10^{14} h^{-1} M_{\odot}$ are taken into account. A value $T = 1.0$ means that the cluster is prolate, $T = 0.0$ indicates that the cluster is oblate. The different panels and curves have the same meaning as in Figure 2.

different values of σ_8 are always consistent with each other for all $\Omega_0 = 1.0$ scenarios (the KS-confidence levels for these scenarios are always larger than 0.23).

The ellipticities within the Abell radius ($r = 1.5 h^{-1}$ Mpc) are somewhat larger than those within $r = 1.0 h^{-1}$ Mpc. The difference is about $\Delta \epsilon_1 \approx 0.05$ and occurs in all scenarios. Qualitatively, such an effect is expected for elongated clusters: the aperture bias, as a result of which the cluster seems more spherical than it actually is (e.g., de Theije *et al.* 1995), is less important for a large aperture radius. The projected position angle is found to change very little with radius (see Section 4.5).

Figure 9 shows the distribution of the triaxiality parameter T for all scenarios. The different curves have the same meaning as in Figure 2. No obvious differences are found in the distribution of T between different scenarios. In all scenarios a large number of clusters have $T = 0.6 - 0.9$, indicating that most clusters are nearly prolate. Perfect oblate clusters ($T = 0.0$) are absent in most scenarios. The low- Ω_0 scenarios contain clusters of slightly larger values of T . The 'strange' distribution of T for the k^{-2} scenario with $\sigma_8 = 0.40$ is probably the result of limited statistics: the number of clusters is only 23 (see Table 2).

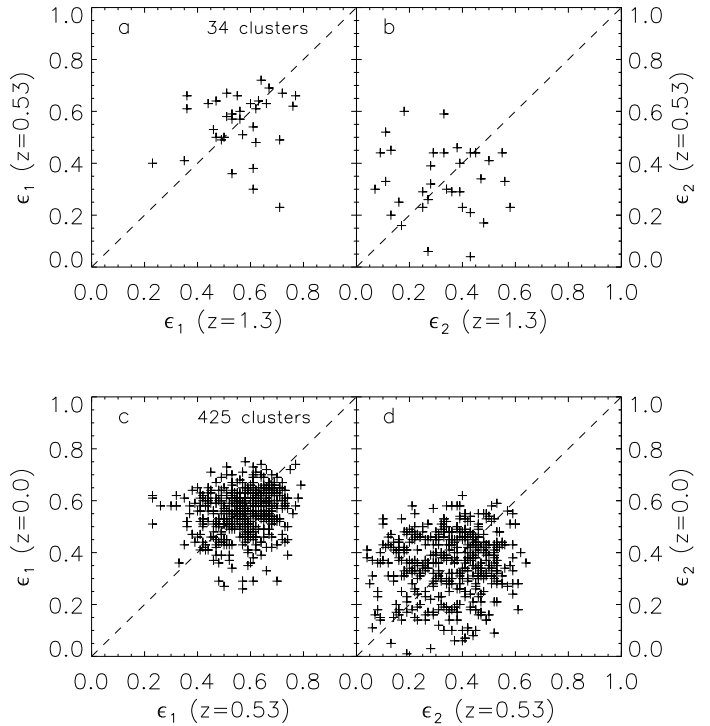


Figure 10. Evolution of the shape of clusters in the hCDM scenario. Only clusters are used that have a mass of at least $2.22 \times 10^{14} h^{-1} M_{\odot}$ at both redshifts. **a:** ϵ_1 at $z = 1.3$ versus $z = 0.53$. **b:** ϵ_2 at $z = 1.3$ versus $z = 0.53$. **c:** ϵ_1 at $z = 0.53$ versus $z = 0$. **d:** ϵ_2 at $z = 0.53$ versus $z = 0$.

4.4.2 Evolutionary changes in ϵ_1 , ϵ_2 and T

The distributions of ϵ_1 for different values of σ_8 in the $\Omega_0 = 1.0$ scenarios in Figure 8 are not significantly different. This does not necessarily mean that individual clusters have a constant ϵ_1 and ϵ_2 . To investigate this, we determine ϵ_1 and ϵ_2 for the clusters in the hCDM scenario at different times, as an example for the $\Omega_0 = 1.0$ scenarios. In Figures 10a and b, the values of ϵ_1 and ϵ_2 at $z = 1.3$ are compared with those at $z = 0.53$. For this, only clusters that fulfil the minimum mass limit at both redshifts are used. We identify the same clusters at both redshifts by requiring that at least half of the particles of the cluster at one redshift is member of the cluster at the other redshift, and vice versa. This uniquely links clusters at different redshifts. The same procedure is repeated for clusters at $z = 0.53$ and $z = 0.0$ (Figures 10c and d). Although the distributions of ϵ_1 and ϵ_2 are roughly constant in time, individual clusters may show large changes. These occur both ways, i.e. ϵ_1 and ϵ_2 can both increase and decrease. The mean change in ϵ_1 between redshifts $z = 1.3$ and 0.53 is 0.00, and the *r.m.s.* scatter around this line is 0.16. Between redshifts $z = 0.53$ and the present, the mean change is -0.01 and the *r.m.s.* scatter is 0.12. For ϵ_2 these values are -0.01 and 0.20 between $z = 1.3$ and 0.53 and 0.00 and 0.25 between $z = 0.53$ and $z = 0.0$, respectively.

For the $\Omega_0 = 0.2$ scenarios, this picture does not change qualitatively, but quantitatively the changes are somewhat smaller. In Figure 11 the same plots are shown as in Fig-

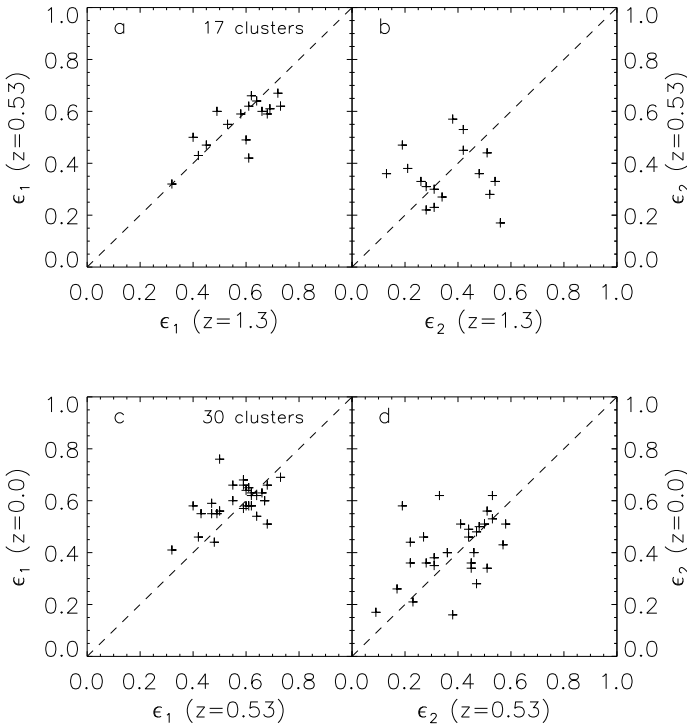


Figure 11. Evolution of the shape of clusters in the LCDMb scenario. Only clusters are used that have a mass of at least $2.22 \times 10^{14} h^{-1} M_\odot$ at both redshifts. The panels have the same meaning as in Figure 10.

ure 10 but now for clusters in the LCDMb scenario. Low- Ω_0 clusters change their ellipticities in the course of time as well, but the dispersions are smaller than in Figure 10. The mean and *r.m.s.* change between $z = 1.3$ and 0.53 are 0.02 and 0.08 for ϵ_1 and 0.01 and 0.17 for ϵ_2 , respectively. Between $z = 0.53$ and 0.0 these values are -0.03 and 0.09 for ϵ_1 and -0.03 and 0.24 for ϵ_2 , respectively. However, one should keep in mind that the number of clusters in the LCDMb scenario is (much) smaller than in the hCDM scenario, especially at later times. The results for the LCDMc and LCDMd scenario are similar to those for the LCDMb scenario.

Combining the results for all scenarios, we conclude that the mean values of $\epsilon_{1,z1} - \epsilon_{1,z2}$, with $z1 \neq z2$, are always consistent with zero. I.e., there is no significant change in the average cluster ellipticities over the time interval studied. The *r.m.s.* values range from about 0.10 (for ϵ_1 and $\Omega_0 < 1.0$) to about 0.25 (for ϵ_2 and $\Omega_0 = 1.0$).

Using the number-selected cluster samples, the results for the changes in ϵ_1 and ϵ_2 are very similar to those for the mass-limited samples.

It is interesting to note that the change in ϵ_2 is always larger than the change in ϵ_1 . This may be caused by the fact that ϵ_2 is always smaller than ϵ_1 [Eqs. (3)], and therefore its determination is somewhat more difficult, as values closer to zero are more difficult to measure (de Theije *et al.* 1995). However, because of the rather large number of particles per cluster, at least $100/\Omega_0$, this cannot account for the whole effect. One possible explanation is the following: a change in b only affects ϵ_2 , whereas a change in c only affects

ϵ_1 . If b and $c(\leq b)$ are fixed, a change in a has a larger influence on ϵ_2 than on ϵ_1 . Quantitatively, if one adopts the mean values $\langle \epsilon_1 \rangle \approx 0.55$ and $\langle \epsilon_2 \rangle \approx 0.35$, one expects on the basis of this simple argument that $\Delta\epsilon_2 = (1 - \langle \epsilon_2 \rangle)/(1 - \langle \epsilon_1 \rangle)\Delta\epsilon_1 \approx 1.4\Delta\epsilon_1$. This is roughly equal to the actual values of $\Delta\epsilon_2/\Delta\epsilon_1$ that are found, though the scatter in $\Delta\epsilon_2/\Delta\epsilon_1$ between different scenarios is rather large ($\Delta\epsilon_2/\Delta\epsilon_1 \approx 1.3 - 2.0$).

For the hCDM scenario the mean and *r.m.s.* changes in T between $z = 1.3$ and 0.53 are -0.02 and 0.29 , respectively. Between $z = 0.53$ and 0.0 these values are -0.02 and 0.25 . For the LCDMb scenario, the mean and *r.m.s.* changes between $z = 1.3$ and 0.53 are -0.02 and 0.20 , respectively, and between $z = 0.53$ and 0.0 these values are -0.03 and 0.17 , respectively. The mean value of $T_{z1} - T_{z2}$, with $z1 > z2$, is negative for all scenarios, which indicates that, on average, T increases with time. That is, clusters become more prolate. This may also be the reason why the $\Omega_0 = 0.2$ model clusters have, on average, a larger value of T . They have evolved further than clusters in an $\Omega_0 = 1.0$ scenario. The *r.m.s.* scatter decreases slightly with time in most scenarios.

Our results, that the values of ϵ_1 and ϵ_2 change in time, while the distribution of ϵ_1 is constant in time, may be explained as follows: at a specific time new particles, that were not within the cluster before, enter the cluster. For an individual cluster, the new cluster particles may enter the cluster via one specific direction and change its shape. However, averaged over the cluster population, the new particles fall in isotropically and therefore do not change the distribution of ellipticities of the cluster population as a whole.

The idea that clusters become more prolate at later times is consistent with the findings of Salvador-Solé & Solanes (1993). They concluded that the elongations of clusters are consistent with clusters being prolate and that the elongations are mainly produced by the tidal interactions of sufficiently massive nearby clusters.

4.5 Alignments

Dekel *et al.* (1984) and West *et al.* (1989) concluded that the relative orientations of cluster major axes with the direction towards neighbouring clusters provide a sensitive test for the formation of large-scale structure in the Universe. However, they used 'only' about 10,000 particles in their simulations, so their results may be influenced by resolution effects. We study this question again, using our simulations in which we measure cluster major axes using the tensor of inertia method (see Section 4.4). We consider here only the alignments in 3-D. The alignments that result in projected 2-D data will be discussed in Paper II. Three types of alignment of a cluster with its environment are investigated.

4.5.1 Alignment with nearest neighbour

The first type of alignment considered is that between the cluster major axis and the direction towards the nearest neighbour cluster. This is the sort of alignment that Binggeli (1982) found observationally in projection. It may arise, e.g., from the tidal force of a neighbouring cluster on the cluster under consideration. Likewise, the filamentary structure of

Table 6. Kolmogorov–Smirnov (KS) confidence levels that the clusters in our simulations do *not* show an alignment effect. The first two columns indicate the scenario and the value of σ_8 . The quantities with the subscript '144' refer to the number-selected cluster samples, whereas all other quantities refer to the mass-limited samples. Columns 3 to 5 give the KS-confidence levels that the cluster major axis is *not* aligned with the direction towards its nearest neighbour. The number of clusters involved in the mass-limited samples is given in column 3. Column 6 to 8 give the KS-confidence levels that the cluster major axis is *not* aligned with the mass distribution within $10h^{-1}$ Mpc around it. The number of clusters involved in the mass-limited samples is given in column 6. Column 9 and 10 give the KS-confidence levels that the cluster major axis is *not* aligned with the major axis of its nearest neighbour cluster. The number of clusters involved in the mass-limited samples is given in column 3. See the text for more details.

scenario	σ_8	$N_{1,3}$	$P_{\text{KS},1}$	$P_{\text{KS},1,144}$	N_2	$P_{\text{KS},2}$	$P_{\text{KS},2,144}$	$P_{\text{KS},3}$	$P_{\text{KS},3,144}$
SCDM	0.46	23	1.00	1.00	78	0.13	0.26×10^{-1}	1.00	0.70
SCDM	0.61	309	0.65	0.57	398	0.79×10^{-6}	0.39×10^{-2}	0.11	0.23
LCDMb	0.90	12	0.85	0.26×10^{-1}	49	0.54×10^{-1}	0.15×10^{-4}	0.97	1.00
LCDMc	0.90	7	0.85	0.34×10^{-1}	47	0.43	0.58×10^{-3}	1.00	1.00
LCDMd	0.90	140	0.32	0.75	179	0.36×10^{-3}	0.92×10^{-3}	0.29	0.20
k^{-2}	0.46	4	0.91	1.00	23	0.55	0.49	0.98	0.78
k^{-2}	0.64	148	0.97	0.99	191	0.30×10^{-3}	0.63×10^{-2}	0.90	1.00
hCDM	0.44	4	1.00	1.00	34	0.65×10^{-1}	0.74×10^{-1}	0.70	0.61
hCDM	0.65	336	0.26	0.36	425	0.24×10^{-7}	0.23×10^{-3}	0.19	0.82
hCDM	1.00	1108	0.66×10^{-6}	0.86×10^{-2}	1168	0.24×10^{-18}	0.11×10^{-2}	0.52	1.00
TCDM	0.47	24	0.29	0.66	81	0.19×10^{-2}	0.40×10^{-3}	1.00	0.60
TCDM	0.60	259	0.93×10^{-2}	0.85×10^{-1}	338	0.91×10^{-7}	0.40×10^{-5}	0.20	0.94
HDM	0.44	0		1.00	35	0.63×10^{-1}	0.84×10^{-2}		0.81
HDM	0.66	303	0.26	0.37	458	0.83×10^{-17}	0.33×10^{-6}	0.18	0.67
HDM	1.00	953	0.20×10^{-9}	0.11×10^{-3}	1063	0.91×10^{-47}	0.44×10^{-7}	0.20×10^{-1}	0.37

the mass (or galaxy) distribution may induce this type of alignment.

The distribution of the angle between the cluster major axis and the direction to its nearest neighbour is shown in Figure 12. In this Figure, only clusters with a mass of at least $2.22 \times 10^{14} h^{-1} M_\odot$ are included, which have a nearest neighbour with a mass of at least $1.00 \times 10^{14} h^{-1} M_\odot$ and which is closer than $20h^{-1}$ Mpc. The results are plotted in terms of $\cos(\Delta\phi)$ because one expects a random distribution to result in a uniform distribution of $\cos(\Delta\phi)$.

There is some dependence of these distributions on the cosmological scenario. However, the differences are rather hard to quantify because of the small number of cluster pairs involved in some of the scenarios. The fourth column of Table 6 gives the confidence levels, derived from a KS-test, that the distribution of $\cos(\Delta\phi)$ is consistent with a random distribution. The third column gives the number of cluster pairs involved in this analysis. All scenarios are consistent with a random distribution, except the hCDM, TCDM and HDM scenarios with the largest value of σ_8 . This could be mainly due to the large number of cluster pairs in these scenarios. If the minimum mass limit for the parent cluster is decreased by a factor of two, the two $\Omega_0 = 0.2$ scenarios show a significant alignment effect as well, while the $\Omega_0 = 0.8$ scenario shows a marginally significant alignment effect. Apparently, the significance is mainly restricted by the number of cluster pairs in the sample. Changing the minimum mass of the nearest neighbour cluster does not influence the above results. Relaxing the constraint that the

nearest neighbour should be within $20h^{-1}$ Mpc of the parent cluster only changes the result for the HDM scenario with $\sigma_8 = 0.66$. The KS-confidence level for this scenario to have a random distribution of $\cos(\Delta\phi)$ then becomes 0.048, a marginally significant alignment.

There is a somewhat stronger cluster alignment if one only considers cluster pairs with distances between 10 and $20h^{-1}$ Mpc.

To check how the above results depend on our definition of the cluster sample, the same analysis is done for the number-selected samples. The results are given in the fifth column of Table 6. All KS-confidence levels are very similar to those in column 4. The significance level is different from that in column 4 only for the $\Omega_0 = 0.2$ scenarios, the hCDM and HDM scenarios with $\sigma_8 = 1.00$, and the TCDM scenario with $\sigma_8 = 0.60$. For the former two scenarios, the alignment effect is just significant for the number-selected catalogues while they were not significant for the mass-limited catalogues. The reason for this difference is the larger number of clusters in the number-selected catalogues.

From the table it appears that the significance of the cluster alignment with respect to its nearest neighbour increases with σ_8 . In other words, the alignment effect gets stronger at later times in the evolution. This can be understood by realizing that it takes some time for the tidal torque of a neighbouring cluster to build up this effect.

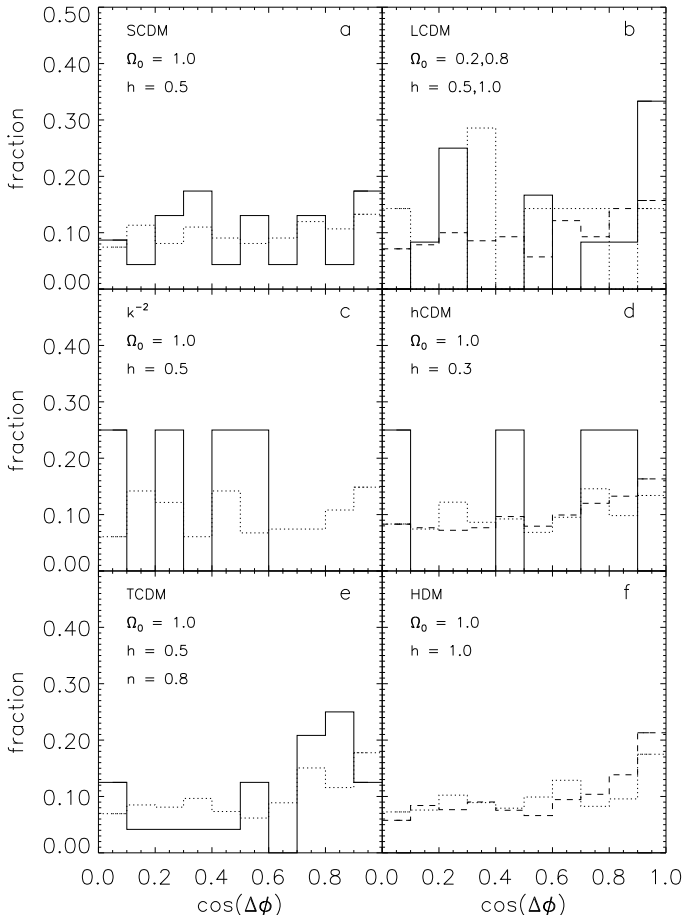


Figure 12. Angle difference between the cluster major axis and the direction to its nearest neighbouring cluster. The distributions are for clusters with a mass of at least $2.22 \times 10^{14} h^{-1} M_\odot$, while the nearest neighbour has a mass of at least $1.00 \times 10^{14} h^{-1} M_\odot$ and is within $20 h^{-1}$ Mpc. The different panels and curves have the same meaning as in Figure 2.

4.5.2 Alignment with environments

The second type of alignment we investigate is that between the cluster major axis and the particle distribution around the cluster. This is similar to the effect described by Argyres *et al.* (1986) and Lambas, Groth & Peebles (1988), who found that galaxy counts are systematically high along the line defined by the projected major axis of a cluster or of its dominant galaxy. The effect extends to at least $15 h^{-1}$ Mpc from the cluster centre.

The distributions of the angle between the cluster major axis and that of the mass distribution within $10 h^{-1}$ Mpc from the cluster are shown in Figure 13. All clusters in the mass-limited cluster catalogues are used for this analysis. There is a significant alignment in almost all scenarios, showing that a cluster is strongly aligned with its surroundings. The alignment is usually much stronger than the alignment of the cluster major axis with its nearest neighbour, which generally is at a distance smaller than $10 h^{-1}$ Mpc. The seventh column in Table 6 gives the KS-confidence levels that the distribution of $\cos(\Delta\phi)$ results from a random orientation. Column 6 gives the number of clusters that is used in this analysis. For almost all $\Omega_0 = 1.0$ scenarios, the signifi-

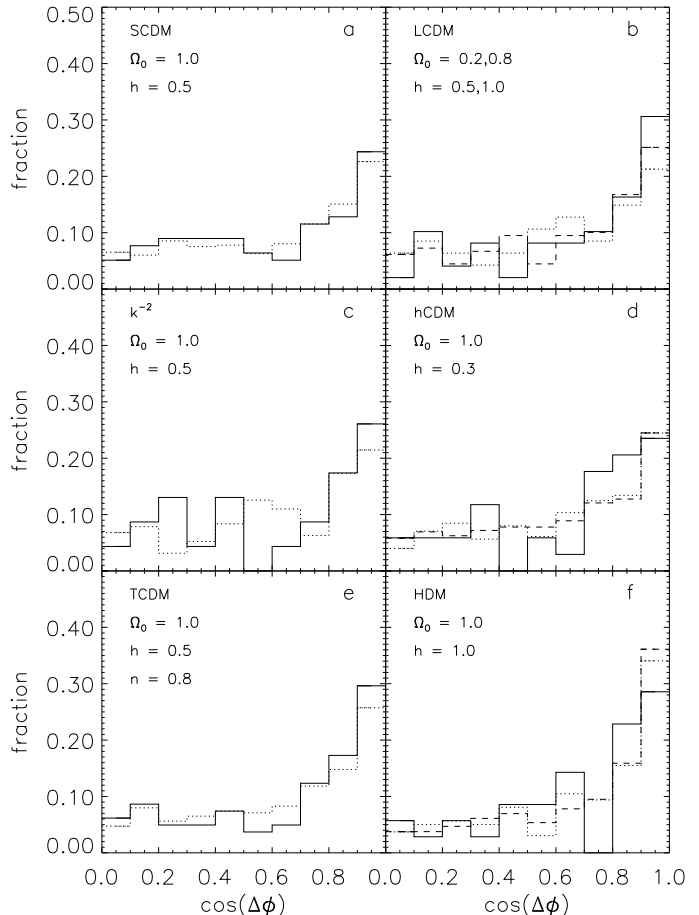


Figure 13. Angle difference between the cluster major axis and the mass distribution within $10 h^{-1}$ Mpc around it. The different panels and curves have the same meaning as in Figure 2.

cance is very high. Only the scenarios with the lowest values of σ_8 have lower significances. The LCDMc scenario does not show a significant alignment effect, while the LCDMb scenario shows some effect. These results may again be somewhat misleading because these scenarios have fewer clusters with masses above the mass limit.

If one uses all particles within $20 h^{-1}$ Mpc of the parent cluster, the alignment signal is still present, though sometimes somewhat less significant. If the surrounding mass distribution in the annulus between 20 and $30 h^{-1}$ Mpc around the cluster is used, only the HDM scenario with $\sigma_8 = 1.0$ shows a positive detection of the alignment.

In column 8 in Table 6 we give the results if the number-selected catalogues are used to do the above analysis instead of the mass-limited catalogues. In this case, almost all scenarios show a significant alignment. Apparently, the significance levels for the mass-limited sample are limited by the small number of clusters used in some cases.

4.5.3 Alignment with nearest neighbour major axis

The third type of alignment that is evaluated is that between the major axes of two neighbouring clusters. This type of alignment is, of course, highly correlated with the first type of alignment that we considered. However, it is not exactly the same. Consider two clusters which are mu-

tual nearest neighbours. If both make an angle of, e.g., 30 degrees with the line connecting them, their relative angle is between 0 and 60 degrees. Furthermore, being a nearest neighbour is not a commutative property. If cluster j is the nearest neighbour of cluster i , but has itself cluster $k \neq i$ as nearest neighbour, then this type of alignment may differ significantly from the first.

As before, only clusters whose mass is larger than $2.22 \times 10^{14} h^{-1} M_{\odot}$, with a nearest neighbour with a mass larger than $1.00 \times 10^{14} h^{-1} M_{\odot}$ and closer than $20 h^{-1}$ Mpc, are taken into account. We find that there is no alignment of major axes of neighbouring clusters. The ninth column in Table 6 gives the KS-confidence levels for the model clusters to show no alignment. The number of cluster pairs involved in this analysis is given in column 3. Lowering the minimum mass limit of the parent cluster by a factor of two does not change this result.

Similarly, the results for this type of alignment do not change if one uses the 144 most massive groups in the simulations. So the previous results are not due to small number statistics. For completeness, the KS-confidence levels for the number-selected sample are shown in column 10 of Table 6.

4.5.4 Overall alignment properties

Summarizing the alignment properties of clusters with their nearest neighbouring clusters and their environments, one may conclude that clusters tend to be strongly aligned with their surrounding mass distribution in almost all scenarios. The alignment with the direction towards their nearest neighbour cluster is less prominent. It is only significant for clusters in the hCDM and HDM scenarios, which have the largest value of σ_8 , and marginally significant in the LCDMb and LCDMc scenarios, both with $\Omega_0 = 0.2$, and the TCDM scenario. The alignment between cluster major axes of nearest neighbours is not significant in any of the scenarios. Even though a cluster may be aligned with the direction towards its nearest neighbouring cluster, this nearest neighbour itself is more likely to be aligned with its immediate surroundings than with the former cluster.

The different strengths of the various types of alignment suggest that although clusters are aligned with their nearest neighbour, they may be rotated around this direction with almost random rotation angles. Note that clusters are not necessarily each others nearest neighbours. For neighbours within $20 h^{-1}$ Mpc, there is only a 52–60% probability that cluster j has cluster i as its nearest neighbour if j is nearest neighbour of i . This probability is almost identical in all scenarios and causes nearest neighbour cluster major axes to be less aligned than the major axis of a cluster with respect to the direction towards its nearest neighbour.

5 RELATIONS BETWEEN COSMOLOGICAL PARAMETERS AND CLUSTER PROPERTIES

Our set of scenarios is chosen in such a way that one can compare scenarios that differ in the value of one cosmological parameter only. The influence of this particular parameter on the cluster properties can then be investigated. One

may even try to get scaling relations which describe the dependence of specific cluster properties on the values of the cosmological parameters. This analysis is complicated by the fact that the clusters themselves can be very different in different scenarios. For example, the clusters that are identified in the $\Omega_0 = 0.2$ scenarios have a much smaller mass than clusters in the $\Omega_0 = 1.0$ scenarios (see Section 4.1). If one wants to investigate the influence of Ω_0 on, e.g., the cluster shape, one can either use the whole cluster sample or only the clusters in a specific mass range. In the former case, the correlation between cluster mass and shape (de Theije *et al.* 1995) will influence the results.

In Table 7 we summarize the parameters of which the effect on cluster properties are investigated. Column 2 gives the probed values of the particular parameter. Column 3 shows the scenarios used for the comparison. As discussed before (Section 2.1), for the spectral parameter Γ we can only compare scenarios for which the value of σ_8 differs as well. So those scenarios will not yield a direct indication of the influence of Γ only, but of the combination of Γ and σ_8 . In this Section, we will only discuss the combinations of cosmological parameters and cluster properties that appear correlated.

5.1 R.m.s. mass fluctuation on scales of $8 h^{-1}$ Mpc, σ_8

When one compares all scenarios which differ only by the value of σ_8 , one finds that a larger value of σ_8 produces a larger number of clusters with a mass of at least $2.22 \times 10^{14} h^{-1} M_{\odot}$ (see Table 2), and that each cluster individually contains more mass. These correlations are consistent with previous findings of, e.g., White, Efstathiou & Frenk (1993) and Eke *et al.* (1996). Using the functional form $N \propto \sigma_8^{c_1+c_2\sigma_8}$ (Eke *et al.* 1996), one obtains $c_1 \approx 5.5 - 6.0$ for all $\Omega_0 = 1.0$ scenarios. The parameter c_2 depends on the scenario and ranges from -5.1 for the HDM scenario to 1.4 for the k^{-2} scenario. Note that an exponential of the form $N \propto \exp(c\sigma_8)$ does not provide a reasonable fit.

For the $\Omega_0 = 1.0$ scenarios, the fraction of high- σ_{los} clusters increases with σ_8 only for the hCDM and HDM scenarios, as does the largest value of σ_{los} . The median value of σ_{los} is constant if one restricts the analysis to clusters in the mass range $1.5 \times 10^{14} h^{-1} M_{\odot} \leq M \leq 2.0 \times 10^{14} h^{-1} M_{\odot}$. This is expected because σ_{los}^2 correlates with M (see Figure 6), and using a fixed and very small mass range will result in clusters which have almost identical values for σ_{los} .

These results are independent of the mass limit that one applies, at least in the range $1.0 - 5.0 \times 10^{14} h^{-1} M_{\odot}$. These results cannot be checked directly for $\Omega_0 < 1.0$ from our scenarios.

If one uses the set of the 144 most massive clusters, the median value of σ_{los} increases with σ_8 for the $\Omega_0 = 1.0$ scenarios and is constant in time for the $\Omega_0 < 1.0$ scenarios. In particular, for the SCDM scenario one gets $\sigma_{\text{los,median}} \propto \sigma_8^{0.90 \pm 0.01}$, for the hCDM scenario $\sigma_{\text{los,median}} \propto \sigma_8^{\approx 0.84 \pm 0.01}$, and for the HDM scenario $\sigma_{\text{los,median}} \propto \sigma_8^{\approx 0.78 \pm 0.01}$. The indicated errors are due to the fitting only.

The particle mass of the clusters increase with σ_8 as well. The fractional increase is about twice as large as for

Table 7. Summary of the cosmological parameters that were varied in the simulations. The first column gives the cosmological parameter. The second column shows the parameter values that were used for investigating the influence of the parameter. The third column gives the identification of the scenarios that are used for the investigation. The fourth to eighth columns show the other parameters that describe a scenario.

parameter	values	scenarios	other parameter values				
			σ_8	Ω_0	spectrum	h	n
σ_8	0.46–0.61	SCDM		1.0	CDM	0.5	1.0
	0.46–0.64	k^{-2}		1.0	k^{-2}	0.5	1.0
	0.44–1.00	hCDM		1.0	CDM	0.3	1.0
	0.47–0.60	TCDM		1.0	CDM	0.5	0.8
	0.44–1.00	HDM		1.0	HDM	1.0	1.0
Ω_0	0.34–1.00	SCDM–LCDMd–LCDM034	≈ 0.60		CDM	0.5	1.0
spectrum	CDM/k^{-2}	SCDM– k^{-2}	0.46–0.61	1.0		0.5	1.0/–2.0
n	1.0/0.8	SCDM–TCDM	0.46–0.61	1.0	CDM	0.5	0.5
h	0.5/0.3	SCDM–hCDM	0.46–0.61	1.0	CDM		1.0
	0.5/1.0	LCDMb–LCDMc	0.90	0.2	CDM		1.0
Γ	0.20–0.43	LCDMc	0.48–0.90	0.2	CDM	1.0	1.0

$\sigma_{\text{los,median}}$, as is expected from the virial theorem. Although this is only shown for the $\Omega_0 = 1.0$ scenarios, White *et al.* (1993) showed that it holds for open scenarios as well. The median value of the cluster particle mass seems to increase significantly with σ_8 only for the hCDM and HDM scenarios. For the hCDM scenario the dependence is given by $M_{\text{median}} \propto \sigma_8^{0.31 \pm 1.58}$ while for the HDM scenario the best-fitting relation is $M_{\text{median}} \propto \sigma_8^{0.33 \pm 0.76}$. The errors in the exponents are so large that the correlations are yet insignificant. For all other scenarios the median value of the cluster particle mass is nearly constant. These results are independent of the mass limit that one applies, at least in the range $1.0 - 5.0 \times 10^{14} h^{-1} M_\odot$. If the number-selected cluster set is used, the results are similar to those for the median value of the cluster velocity dispersion. For the SCDM scenario $M_{\text{median}} \propto \sigma_8^{1.63 \pm 0.46}$, for the hCDM scenario $M_{\text{median}} \propto \sigma_8^{1.48 \pm 0.61}$, and for the HDM scenario $M_{\text{median}} \propto \sigma_8^{1.41 \pm 1.01}$. For the low- Ω_0 scenarios the median value of the cluster particle mass is constant in time.

A larger σ_8 produces larger cluster peculiar velocities (see Table 5). The dispersion of the best-fitting Gaussian distribution to the 1-D cluster peculiar velocity distribution scales, on average, linearly with σ_8 , with a scatter of about 10%. This linear relation is identical to that predicted by linear perturbation theory ($v_{\text{pec}} \propto \Omega^{0.6} \sigma_8$; e.g., Peebles 1993).

The normalization σ_8 has a large effect on the alignment properties of clusters. Especially the alignment of a cluster with its nearest neighbour and with the surrounding mass distribution are influenced by σ_8 (see Table 6). Scenarios with a larger value of σ_8 contain clusters that are better aligned both with the direction towards their nearest neighbour and with their surroundings.

5.2 Density parameter Ω_0

Comparing the SCDM scenario with $\sigma_8 = 0.61$ with the LCDMd scenario, it is clear that a higher value of the density parameter Ω_0 will produce more clusters with a mass of at least $2.22 \times 10^{14} h^{-1} M_\odot$. To quantify this, we also include the LCDMb scenario at the epoch where $\sigma_8 \approx 0.6$. This is between $a_{\text{exp}} = 0.44$ and $a_{\text{exp}} = 0.55$, and the value of Ω is then equal to 0.34. We will refer to this scenario as LCDM034 from now on. The number of clusters with a mass of at least $2.22 \times 10^{14} h^{-1} M_\odot$ is about 23 in this scenario. Using the functional form $N \propto \Omega^{c_1 + c_2 \Omega}$ to describe the number of clusters with a mass of at least $2.22 \times 10^{14} h^{-1} M_\odot$, analogous to Eke *et al.* (1996), one obtains $c_1 = 1.95$ and $c_2 = 2.09$. An exponential of the form $N \propto \exp(c \Omega_0)$ does not provide a good fit.

The density parameter influences the velocity dispersion of clusters above a certain mass. This can be seen in Figure 14a. The difference in $\rho(> \sigma_{\text{los}})$ between the SCDM and LCDMd scenarios is not very significant, but that between the SCDM and LCDM034 scenarios is. The latter lacks the high- σ clusters that the SCDM scenario contains. If one uses only the 144 most massive groups in both scenarios one finds that the velocity dispersions of these are larger for higher Ω_0 , $\sigma_{\text{los,median}} \propto \Omega_0^{\approx 0.5}$.

Figure 14b shows the cumulative distribution of cluster mass for the SCDM, LCDMd and LCDM034 scenarios for all clusters in the mass-limited catalogues. All distributions are scaled to the same number of clusters. The SCDM scenario has a few clusters that have a somewhat larger mass than the most massive clusters in the LCDMd scenario. The curve for the LCDMd scenario is systematically, though only slightly, below that of the SCDM scenario. This is consistent with the findings of, e.g., White *et al.* (1993). The same conclusions hold if one compares the SCDM scenario with the LCDM034 scenario, but the differences are then even larger. If one uses

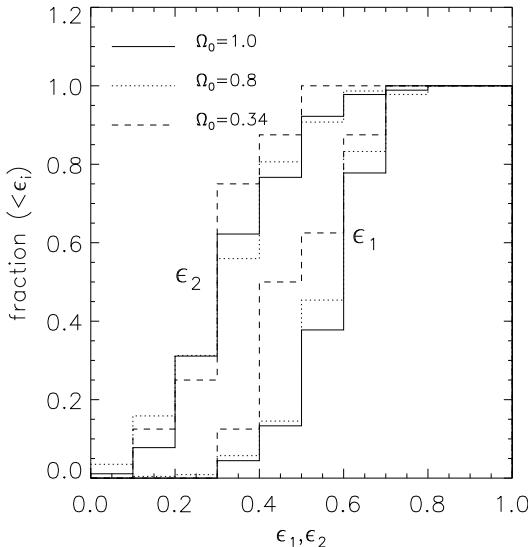


Figure 15. Cumulative distributions of cluster ellipticity ϵ_1 (heavy lines) and ϵ_2 (thin lines) for the SCDM scenario (solid lines, 90 clusters), the LCDMd scenario (dotted lines, 227 clusters) and the LCDM034 model (dashed lines, 8 clusters). Only clusters that have a mass in the range $(1.5 - 2.0) \times 10^{14} h^{-1} M_\odot$ are used. The mean values of ϵ_1 are 0.62, 0.60 and 0.53 for the SCDM, LCDMd and LCDM034 scenarios, respectively.

the number-selected catalogues in both scenarios, the cluster mass is largest for the $\Omega_0 = 1.0$ scenario (see Figure 2). The median value of the cluster particle mass for clusters in the number-selected sample scales as $M_{\text{median}} \propto \Omega_0^{0.8}$.

In Figure 14c we show the distributions over 3-D ellipticities for the SCDM, LCDMd and LCDM034 scenarios and for clusters above the mass limit of $2.22 \times 10^{14} h^{-1} M_\odot$. No significant differences between these distributions are detected. This may seem surprising because previous studies showed that the cluster ellipticity *increases* with Ω_0 (Mohr *et al.* 1995, de Theije *et al.* 1995). However, the mass range involved here differs substantially between the different scenarios (see Section 2.2.2). As was pointed out by Struble & Ftaclas (1994) and de Theije *et al.* (1995), the more massive clusters are less elongated than the less massive ones. This anti-correlation between ϵ and M is also detected in the present simulations.

To investigate whether ϵ_1 and ϵ_2 are smaller for clusters in low- Ω_0 scenarios when clusters of the same mass are considered, we show in Figure 15 the cumulative distributions of ϵ_1 (heavy lines) and ϵ_2 (thin lines) for the SCDM scenario with $\sigma_8 = 0.61$, the LCDMd scenario (having $\sigma_8 = 0.60$) and the LCDM034 scenario (having $\sigma_8 \approx 0.60$). These scenarios differ only in the value of Ω_0 . Only clusters in the mass range $1.5 \times 10^{14} h^{-1} M_\odot \leq M \leq 2.0 \times 10^{14} h^{-1} M_\odot$ are included. This is to eliminate the correlation between ϵ_i and M . It is clear that clusters in the same mass range are less flattened in the $\Omega_0 = 0.8$ scenario than in the $\Omega_0 = 1.0$ scenario, consistent with the previous findings of Mohr *et al.* (1995) and de Theije *et al.* (1995). The mean values of ϵ_1 are 0.62, 0.60 and 0.53 for the SCDM, LCDMd and LCDM034 scenarios, respectively, with dispersions of 0.10, 0.11 and 0.13.

The mean values of ϵ_2 are 0.39, 0.38 and 0.34, respectively, with dispersions of 0.15, 0.16 and 0.11. Interpolating linearly, we find $\langle \epsilon_1 \rangle = 0.48 + 0.13 \Omega_0$ and $\langle \epsilon_2 \rangle = 0.31 + 0.08 \Omega_0$ for clusters in the same mass range.

The dispersions of the fitted Gaussian distributions to the distributions of cluster peculiar velocity indicate that a somewhat smaller value of Ω_0 results in slightly smaller cluster peculiar velocities, consistent with previous work of, e.g., Bahcall *et al.* (1994) and Gramann *et al.* (1995). The difference in dispersions between the SCDM and LCDMd scenarios is 28 km s^{-1} , or about 13%, while the difference between the SCDM and LCDM034 scenarios is 42 km s^{-1} , or about 17%. As linear perturbation theory predicts a relation $v_{\text{pec}} \propto \Omega^{0.6}$ for constant σ_8 (e.g., Peebles 1993), we fit the power-law relation $\sigma_{\text{pec},1D} \propto \Omega^\gamma$. This does not provide a good fit. Neither does an exponential $\sigma_{\text{pec},1D} \propto \exp(b \Omega_0)$ give an acceptable fit.

5.3 Spectrum

Comparing the SCDM with the k^{-2} scenario, both with $\sigma_8 = 0.46$ or with $\sigma_8 \approx 0.61 - 0.64$, one finds that the number density of clusters is about twice as large for the SCDM scenario as for the k^{-2} scenario. The SCDM spectrum has more power on scales less than $8h^{-1} \text{ Mpc}$, as its effective power law index in this k -region is -1 . Apparently, this extra power on the somewhat smaller ($\approx 2h^{-1} \text{ Mpc}$) scales stimulates cluster formation considerably through merging of smaller clumps.

The comparison between the SCDM and k^{-2} scenarios with $\sigma_8 = 0.61 - 0.64$ is shown in Figure 16. The line-of-sight velocity dispersions are slightly larger for the k^{-2} scenario. The differences in cluster mass between both scenarios are larger. Clusters in the k^{-2} scenario have larger masses than those in the SCDM scenario.

The shape of the power spectrum has some influence on the distribution over ellipticities. The ellipticities for the SCDM spectrum are somewhat larger than those for the k^{-2} -spectrum, especially for $\sigma_8 \approx 0.61 - 0.64$. The KS-confidence levels for both distributions to be the same are 0.19 (for ϵ_1) and 0.24 (for ϵ_2) for $\sigma_8 = 0.46$, and 3.6×10^{-3} (for ϵ_1) and 1.1×10^{-5} (for ϵ_2) for $\sigma_8 \approx 0.61 - 0.64$. The latter are thus significant. If one uses the 144 most massive groups in both scenarios, the KS-confidence levels are very similar to those for the mass-limited samples.

The shape of the power spectrum has a significant effect on the cluster peculiar velocity. For the k^{-2} scenario, the cluster peculiar velocity is almost twice as large as for the SCDM scenario. This is due to the extra power of the k^{-2} scenario on the very large scales. The results for the number-selected samples are the same.

The index of the primordial spectrum n only has some influence on the cluster number densities and peculiar velocities. For the number densities, the number of clusters scales as $N \propto n^\delta$, with $\delta \approx 1.0$, although for various values of σ_8 the value of δ varies from 0.8 to 1.2. The peculiar velocity is larger by about 20 km s^{-1} (or about 8%) for the TCDM scenario with $n = 0.8$, due to the extra large-scale power. Using the functional form $\sigma_{\text{pec},3D} \propto n^{-\tau}$ one gets $\tau = 0.41 \pm 0.20$. Because n does not correlate strongly with the cluster properties, its value can be chosen in order to fit

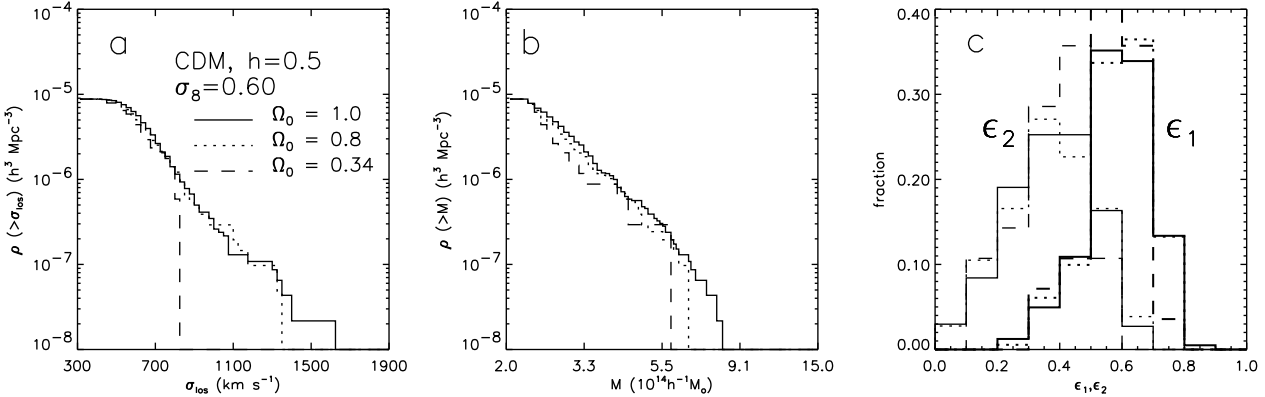


Figure 14. **a:** Cumulative distribution of cluster velocity dispersion for the SCDM scenario with $\sigma_8 = 0.61$ ($\Omega_0 = 1.0$, solid line), the LCDM_d scenario ($\Omega_0 = 0.8$, dotted line) and the LCDM₀₃₄ scenario ($\Omega_0 = 0.34$, dashed line). Only clusters in the mass-limited samples are included and all three distributions have been scaled to a total cluster density of $8.6 \times 10^{-6} h^3 \text{ Mpc}^{-3}$. **b:** Same as **a**, but for cluster masses. **c:** Distributions of cluster ellipticities. The heavy lines are the distributions of ϵ_1 , whereas the thin lines indicate the distributions of ϵ_2 . Only clusters with a mass of at least $2.22 \times 10^{14} h^{-1} M_\odot$ are used. The curves have the same meaning as in panel **a**.

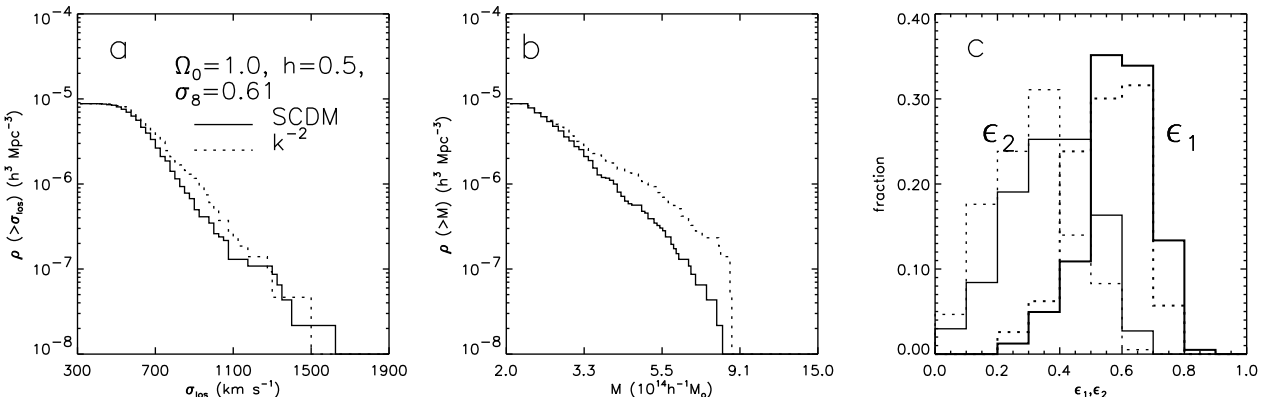


Figure 16. Same as Figure 14. The solid line is for the SCDM scenario with $\sigma_8 = 0.61$ and the dotted line is for the k^{-2} scenario with $\sigma_8 = 0.64$.

the COBE data. Cen *et al.* (1992) found that $n = 0.7 - 0.8$ is the most interesting range.

5.4 Hubble parameter h

For the SCDM and hCDM scenarios with $\sigma_8 \approx 0.61 - 0.65$ and for the LCDM_d and LCDM_c scenarios, the number of clusters with a mass of at least $2.22 \times 10^{14} h^{-1} M_\odot$ is almost identical, so h does not have a large influence on the cluster number densities. Of course, there would be a large difference in the number of clusters if one would express the mass of a cluster in units of M_\odot instead of $h^{-1} M_\odot$. In that case, the LCDM_d scenario would have 201 clusters with $M > 2.22 \times 10^{14} M_\odot$. Qualitatively, this is expected as the Universe is twice as old for the LCDM_d scenario as it is for the LCDM_c scenario (see the last column of Table 1). Using only the comparison between the LCDM_d and LCDM_c scenario, one finds that the number of clusters with a mass of at least $2.22 \times 10^{14} M_\odot$ scales as $N \propto h^{-\alpha}$, with α increasing monotonically from 0.49 at $a_{\text{exp}} = 0.55$ to 2.29 at $a_{\text{exp}} = 1.00$.

A lower value of h results in slightly larger cluster peculiar velocities (see Table 5). This is especially true if σ_8 is not too high, i.e., $\sigma_8 \leq 0.6$. For the dispersion of the 3-D peculiar velocity distribution we find the empirical relation $\sigma_{\text{pec},3D} \propto h^{-\beta}$, where $\beta \approx 0.25 - 0.35$.

The influence of h on the cluster properties is similar if one uses the 144 most massive groups.

5.5 Spectral parameter Γ

The number of clusters with mass larger than $2.22 \times 10^{14} h^{-1} M_\odot$ decreases with increasing Γ . For the LCDM_c scenario one gets $N \propto \Gamma^{-1.55 \pm 0.02}$, though one has to keep in mind that the value of σ_8 changes as well, from 0.47 to 0.90. The actual relation between N and Γ may thus be even steeper. A similar result holds for the LCDM_d scenario, $N \propto \Gamma^{-1.43 \pm 0.01}$.

The median values of the cluster particle mass and velocity dispersion hardly change with Γ for the LCDM_d and LCDM_c models.

The peculiar velocities increase with Γ according to

$\Gamma^{0.32 \pm 0.01}$ for the LCDMc scenario, and according to $\Gamma^{0.38 \pm 0.01}$ for the LCDMb scenario. This is surprising, as a larger Γ means that there is less large-scale power (Efstathiou *et al.* 1992). Furthermore, for the epochs where Γ is smaller, σ_8 is larger. This would suggest an even steeper increase of the peculiar velocity towards the epochs when Γ is small. Possibly the results are influenced by the rather small number of clusters.

6 CONCLUSIONS AND DISCUSSION

The aim of this paper was fourfold: (1) Present the set of simulations which will be used in Paper II to select the scenario that is most consistent with the observations. (2) Study the intrinsic properties of clusters of galaxies for different cosmological scenarios. (3) Investigate which cosmological parameters have the largest influence on these cluster properties. (4) Obtain scaling relations between the cosmological parameters and the cluster properties. These scaling relations can be used to 'interpolate' between existing scenarios.

The following conclusions may be drawn from the present analysis, for the range of parameters studied and the scenarios studied:

- σ_8 (in the range 0.44–1.00):

- The normalization σ_8 correlates positively with the cluster number density, as is expected. This is consistent with the earlier findings of, e.g., White *et al.* (1993). Fitting $N \propto \sigma_8^{c_1+c_2 \sigma_8}$, we get $c_1 \approx 5.5 - 6.0$ for all $\Omega_0 = 1.0$ scenarios, while c_2 differs between various scenarios.
- The median value of the cluster line-of-sight velocity dispersions is almost independent of σ_8 for the $\Omega_0 = 1.0$ scenarios. Only for the hCDM and HDM scenarios there is a slight correlation, although the errors are large. These results are independent of the mass limit that one applies, at least in the range $1.0 - 5.0 \times 10^{14} h^{-1} M_\odot$. Using the number-selected cluster samples, $\sigma_{\text{los,median}} \propto \sigma_8^{0.78-0.90}$ for the $\Omega_0 = 1.0$ scenarios.
- The median value of the cluster particle mass increases somewhat with σ_8 for the hCDM and HDM scenarios, though the errors are very large. These results are independent of the mass limit that one applies, at least in the range $1.0 - 5.0 \times 10^{14} h^{-1} M_\odot$. Using the number-selected cluster samples, $M_{\text{median}} \propto \sigma_8^{1.41-1.63}$.
- The value of σ_8 does not influence the cluster ellipticities. Although for individual clusters the ellipticity changes, the *distribution* of ellipticity is independent of σ_8 .
- A larger value of σ_8 results in significantly larger cluster peculiar velocities. Empirically, we found $\sigma_{\text{pec,1D}} \propto \sigma_8$, as is predicted by linear theory.
- σ_8 does affect the cluster alignment with its nearest neighbouring cluster and with its surroundings. The angle between the major axes of neighbouring clusters does not, or only marginally, depend on σ_8 .

- Ω_0 (in the range 0.34–1.00):

- A larger value of Ω_0 results in an increase in the number of clusters. Fitting the functional form $N \propto \Omega_0^{c_1+c_2 \Omega_0}$ we obtained $c_1 = 1.95$ and $c_2 = 2.09$. Changing Ω_0 changes the shape of the distribution of cluster line-of-sight velocity dispersions for clusters above a certain mass, and it results in considerably larger velocity dispersions for the 144 most massive clusters, $\sigma_{\text{los,median}} \propto \Omega_0^{0.39 \pm 0.08}$.
- A larger Ω_0 produces more high-mass clusters both in absolute and in relative sense, consistent with earlier results of White *et al.* (1993) and Jing & Fang (1994). This holds for both the mass-limited and the number-selected cluster catalogues. For the latter catalogues, $M_{\text{median}} \propto \Omega_0^{0.97 \pm 0.20}$.
- A low value of Ω_0 produces more spherical clusters for a specific mass range. This was already concluded by de Theije *et al.* (1995) and Mohr *et al.* (1995). However, for the sample of clusters above a minimum mass threshold or for the sample of the N most massive clusters, the correlation between Ω_0 and ϵ disappears. This is because the cluster mass is very different in the different scenarios, and because ϵ and M are anti-correlated.
- A larger value of Ω_0 results in an increase in the cluster peculiar velocity, consistent with earlier findings of, e.g., Bahcall *et al.* (1994). However, a fit of the form $\sigma_{\text{pec,1D}} \propto \Omega_0^\gamma$ as is predicted by linear theory, where $\gamma = 0.6$, does not provide a good representation.
- Spectrum (SCDM versus k^{-2}):
- The shape of the spectrum clearly influences the cluster number density. The SCDM spectrum produces more clusters than does the k^{-2} spectrum. The clusters in both scenarios have a similar velocity dispersion.
- The spectrum has some influence on cluster mass as well. Clusters in the k^{-2} scenario have a larger mass than in the SCDM scenario.
- The SCDM spectrum produces clusters that are somewhat more elongated than does the k^{-2} power spectrum. The difference is only significant for $\sigma_8 \geq 0.6$.
- The k^{-2} spectrum produces cluster peculiar velocities that are almost twice as large as for the SCDM spectrum. This is due to the extra power on large scales.
- For smaller values of n , the cluster peculiar velocity is larger because of the extra power on large scales.
- h (in the range 0.5–1.0):
- The Hubble-parameter h affects the cluster peculiar velocity slightly: the 3-D cluster peculiar velocities scale as $h^{-\beta}$, with $\beta \approx 0.25 - 0.35$. This is because for smaller values of h the Universe is older.
- Γ (in the range 0.20–0.43):
- The number of clusters decreases with Γ according to $N \propto \Gamma^{-1.55 \pm 0.02}$ for the LCDMc scenario, though one should keep in mind that the different scenarios that are used do also have a different value of σ_8 .

- The cluster peculiar velocity scales as $\Gamma \approx 0.32 \pm 0.01$ for the LCDMc scenario and as $\Gamma \approx 0.38 \pm 0.01$ for the LCDMb scenario. This is quite surprising as a larger Γ indicates *less* large-scale power.

In summary, we conclude that σ_8 has the largest influence on the cluster properties. This is not surprising because the mass within the virial radius of a rich cluster is very close to the mass enclosed within a sphere of $8h^{-1}$ Mpc in the unperturbed Universe (e.g., Evrard 1989). Almost all cluster properties change if σ_8 is varied. Ω_0 has a large impact on the cluster number density, mass, and peculiar velocity. In addition, for the number-selected cluster set, relatively more high- σ_{los} clusters are expected if Ω_0 is larger. More power on larger scales produces somewhat more elongated clusters and larger cluster peculiar velocities. The other parameters, the spectrum and h , correlate less strongly with the cluster properties.

The cluster peculiar velocity is the cluster property that depends on the largest number of parameters of the fluctuation scenario. Two difficulties affect the determination of the most consistent cosmological scenario purely on the basis of cluster peculiar velocities. First, the large sensitivity of cluster peculiar velocities on all cosmological parameters make it very hard to disentangle these parameters and determine each of them separately. Fortunately, quite a few relations between cosmological parameters are known from other studies. E.g., Big Bang Nucleosynthesis and the fact that clusters cannot consist of more than 100% baryons put severe limits on the Hubble parameter h as a function of Ω_0 (David, Jones & Forman 1995). Secondly, cluster peculiar velocities are very hard to determine observationally. Mould *et al.* (1991, 1993), e.g., quoted errors of 300 to 800 km s $^{-1}$. Different studies sometimes yielded very different values for v_{pec} for the same cluster. Very recently, Giovanelli *et al.* (1997) obtained the peculiar velocities for a sample of 22 groups and clusters. Although the sample is rather small, the uncertainties are considerably smaller (about 150 km s $^{-1}$) than those in previous studies and it will be very worthwhile to extend this data set to a larger number of clusters.

As the cluster number density depends on the normalization σ_8 , on the density parameter Ω_0 and on the shape of the power spectrum, it can be used to discriminate between different scenarios (White *et al.* 1993, Eke *et al.* 1996). However, the cluster number density in the simulations depends on the exact definition of a cluster. The most straightforward definition is, of course, to apply a mass threshold and consider all objects with a mass larger than this threshold to be clusters. But it is hard to get a reliable mass estimate of a cluster from galaxy positions and velocities. Better mass estimates may be obtained from X-ray measurements and gravitational lensing. Another way to define a cluster may be to use the cluster line-of-sight velocity dispersion and use only those objects which have a σ_{los} larger than some well-chosen value. With the large redshift surveys coming up in the very near future, and with the ENACS-survey (Katgert *et al.* 1996) already being completed, this may prove to be a suitable manner to define a cluster. However, one does not necessarily pick out the most massive objects because of the scatter in the $\sigma_{\text{los}} - M$ -relation (see Figure 6).

It is promising to note that most of the cluster prop-

erties discussed do not depend critically on the cluster definition. That is, most results are qualitatively the same for the mass-limited and the number-selected cluster sample. However, when comparing to observations one should try to construct a model cluster catalogue that is complete in, e.g., richness or X-ray temperature.

In Paper II, we will compare the properties of the 144 most massive clusters in the simulations with many observations. We then try mimic as closely as possible the way in which real clusters are observed. The results of the comparison with observations, together with the results of other studies, can then be used to find the cosmological scenario which is most consistent with all cluster properties. If necessary, the scaling relations can be used to 'interpolate' between scenarios. For the best-fitting scenario, a higher resolution cluster catalogue can then be constructed for which each cluster will be simulated individually at high resolution.

Acknowledgments

We are grateful to Edmund Bertschinger for providing us with his P³M-code, to the National Computing Facility and SARA Amsterdam for giving us a large amount of computing time on the Cray C90. We also wish to thank Frank Robijn and SARA Amsterdam for providing us with extra computing time that made it possible to run an extra scenario. Furthermore, Peter Katgert and Tim de Zeeuw are acknowledged for reading earlier versions of this manuscript and for many useful suggestions. EvK acknowledges an European Community Research Fellowship as part of the HCM program.

REFERENCES

Argyres P. C., Groth E. J., Peebles P. J. E., Struble M. F., 1986, AJ, 91, 471
 Bahcall N. A., Gramann M., Cen R., 1994, ApJ, 436, 23
 Bardeen J. M., Bond J. R., Kaiser N., Szalay A. S., 1986, ApJ, 304, 15
 Beers T. C., Flynn K., Gebhardt K., 1990, AJ, 100, 32
 Bertschinger E., Gelb J. M., 1991, Computers in Physics, 5, 164
 Binggeli B., 1982, A&A, 107, 338
 Buote D. A., Canizares C. R., 1996, ApJ, 457, 565
 Carlberg R. G., Couchman H. M. P., Thomas P. A., 1990, ApJL, 352, L29
 Cen R., Gnedin N. Y., Kofman L. A., Ostriker J. P., 1992, ApJ, 399, L11
 Cen R. Y., Ostriker J., 1992, ApJL, 399, L113
 Crone M. M., Geller M. J., 1995, AJ, 110, 21
 David L. P., Jones C., Forman W., 1995, ApJ, 445, 578
 Dalton G., Croft R. A. C., Efstathiou G., Sutherland W. J., Maddox S. J., Davis M., 1994, MNRAS, 271, L47
 Davis M., Efstathiou G., Frenk C. S., White S. D. M., 1985, ApJ, 292, 371
 Dekel A., West M. J., Aarseth S. J., 1984, ApJ, 279, 1
 den Hartog R., Katgert P., 1996, MNRAS, 279, 349
 de Theije P. A. M., Katgert P., van Kampen E., 1995, MNRAS, 273, 30
 de Theije P. A. M., van Kampen E., Slijkhuis R. G., 1997, submitted to MNRAS (Paper II)
 Efstathiou G., Bond J. R., White S. D. M., 1992, MNRAS, 258,

Efstathiou G., Davis M., Frenk C. S., White S. D. M., 1985,
ApJS, 57, 241

Einasto J., Saar E., Einasto M., Freudling W., Gramann M.,
1994, ApJ, 429, 465

Eke V. R., Cole S., Frenk C. S., 1996, astro-ph/9601088

Evrard A. E., 1989, ApJ, 341, L71

Franx M., Illingworth G., de Zeeuw T., 1990, ApJ, 383, 112

Frenk C. S., White S. D. M., Efstathiou G., Davis M., 1990,
ApJ, 351, 10

Giovanelli R., Haynes M. P., Chamaraux P., da Costa L. N.,
Freudlin W., Salzer J. J., Wegner G., 1997, AJ in press

Gramann M., Bahcall N. A., Cen R., Gott J. R., 1995, ApJ,
441, 449

Heisler J., Tremaine S., Bahcall J. N., 1985, ApJ, 298, 8

Henry J. P., Briel U. G., Nulsen P. E. J., 1993, A&A, 271, 413

Jing Y. P., Börner G., 1995, astro-ph/9508104

Jing Y. P., Fang L. Z., 1994, ApJ, 432, 438

Katgert P., Mazure A., Jones B., den Hartog R., Biviano A.,
Dubath P., Escalera E., Focardi P., Gerbal D., Giuricin G.,
Le Fèvre O., Moles O., Perea J., Rhee G., 1996, A&A, 310, 8

Lambas D. G., Groth E. J., Peebles P. J. E., 1988, AJ, 95, 996

Loveday J., Peterson B. A., Efstathiou G., Maddow S. J., 1992,
ApJ, 390, 338

Lubin L., Bahcall N., 1993, ApJL, 415, L17

Mazure A., Katgert P., den Hartog R., Biviano A., Dubath P.,
Escalera E., Focardi P., Gerbal D., Giuricin G., Jones B., Le
Fèvre O., Moles O., Perea J., Rhee G., 1996, A&A, 310, 31

Mohr J. J., Evrard A. E., Fabricant D. G., Geller M. J., 1995,
ApJ, 447, 8

Mould J. R., Staveley-Smith L., Schommer R. A., Bothun G.
D., Hall P. J., Han M. S., Huchra J. P., Roth J., Walsh W.,
Wright A. E., 1991, ApJ, 383, 467

Mould J. R., Akeson R. L., Bothun G. D., Han M., Huchra J.
P., Roth J., Schommer R. A., 1993, ApJ, 409, 14

Nichol R. C., Briel U. G., Henry J. P., 1994, MNRAS, 267, 771

Nolthenius R., Klypin A., Primack J. R., 1994, ApJ, 422, L45

Padmanabhan T., 1993, Structure Formation in the Universe,
Cambridge University Press

Peebles P. J. E., 1993, Principles of Physical Cosmology,
Princeton University Press

Press W. H., Flannery B. P., Teukolsky S. A., Vetterling W. T.,
1989, Numerical Recipes, Cambridge University Press

Rhee G. F. R. N., van Haarlem M. P., Katgert P., 1989, A&AS,
91, 513

Salvador-Solé E., Solanes J. M., 1993, ApJ, 417, 427

Sarazin C. L., 1986, Rev. Mod. Phys., 58, No. 1

Schindler S., 1996, A&A, 305, 858

Smail I., Ellis R. S., Fitchett M. J., Edge A. C., 1995, MNRAS,
273, 277

Squires G., Kaiser N., Babul A., Fahlman G., Woods D.,
Neumann D. M., Böhringer H., 1996, ApJ, 461, 572

Struble M. F., Ftaclas C., 1994, AJ, 108, 1

Sugiyama N., 1995, ApJSS, 100, 281

Tyson J. A., Fischer P., 1995, ApJ, 446, L55

van Haarlem M. P., Frenk C. S., White S. D. M., 1997,
MNRAS, in press

van Kampen E., 1994, PhD Thesis, Leiden

van Kampen E., 1995, MNRAS, 273, 295

van Kampen E., Katgert P., 1997, submitted

West M. J., Dekel A., Oemler A., 1989, ApJ, 336, 46

White S. D. M., Efstathiou G., Frenk C. S., 1993, MNRAS, 262,
1023

White S. D. M., Frenk C. S., Davis M., Efstathiou G., 1987,
ApJ, 313, 505

Wilson G., Cole S., Frenk C. S., 1996, submitted to MNRAS

